DESIGN OF AN MR-SAFE HAPTIC WRIST MANIPULATOR FOR MOVEMENT DISORDER DIAGNOSTICS

ENABLING SIMULTANEOUS ANALYSIS OF THE CENTRAL AND PERIPHERAL COMPONENTS OF MOVEMENT DISORDER

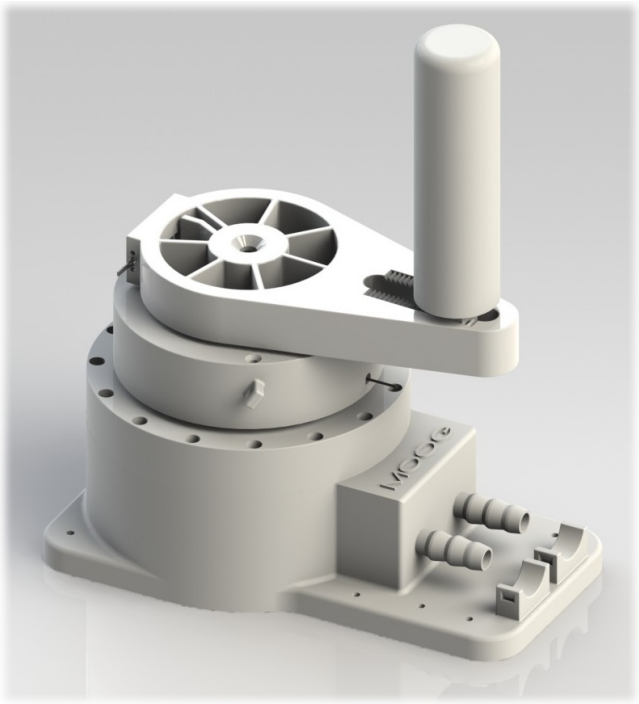

MASTER THESIS

C.H.D. Bode
Student number: wb1192760
Department number: 1321

Supervisors TU Delft:
dr. ir. W. Mugge
dr. ir. A.C. Schouten
prof. dr. F.C.T. van der Helm

Supervisor Moog:
ir. P. Lammertse

14 February 2012

TU Delft Delft University of Technology

MOOG

MASTER THESIS

Name:	C.H.D. Bode
Student number:	wb1192760
Department number:	1321
MSc:	Biomedical Engineering
Specialization:	BioMechatronics (BM)
Supervisors TU Delft:	dr. ir. W. Mugge
	dr. ir. A.C. Schouten
	prof dr. F.C.T. van der Helm
Supervisor Moog:	ir. P. Lammertse

MASTER EXAM - TUESDAY 14 FEBRUARY 2012

Exam committee:	prof. dr. F.C.T. van der Helm, BMechE, 3ME
	ir. J. Meuleman, MOOG
	dr. G.A. Delgado Lopes, Intelligent Control & Robotics, DCSC
	dr. ir. A.C. Schouten, BMechE, 3ME
	dr. ir. W. Mugge, BMechE, 3ME

Preface

Before you lies my master thesis as conclusion of the Master Biomedical Engineering at the faculty of Mechanical, Maritime and Materials Engineering of the Delft University of Technology. My graduation project was to design an MR-compatible haptic wrist manipulator.

The first step taken in designing the manipulator was by making a literature survey on current design solutions for an 1 DOF MR-compatible haptic manipulator. The requirements for the manipulator were drafted and with the results from this survey the best suited solutions for actuation and sensing were determined. Based on these solutions a design was made for an MR-safe electro-hydraulic closed circuit actuator with a custom-build vane motor and MR-safe optical sensors for position and torque. The first prototype for the vane motor was personally made in the student workshop (3ME, Delft). This prototype was tested in a setup with a tube length of 1.5 m to see if the concept proved viable. The result was positive and the setup modified to accommodate tubes with a length of 9 m. The modified setup showed that the prototype suffered from stick-slip friction and that the used tubes were too compliant. Next a visit was undertaken to the medical product development company *Baat Medical* (Hengelo) and the *University of Twente* (Enschede) to discuss their design of a vane motor currently used in research there. With the insights of the first prototype and visit, a new design was made for the vane motor with a dual vane and modified sealing to reduce stick-slip friction. The new design for the vane motor and the designs for the sensors were then used to manufacture parts for a new complete system prototype. This complete system prototype was then tested and its performance determined. Finally a test in the MR-scanner (AMC, Amsterdam) showed no distortions in the MR-image or distortions in the sensor signal from the manipulator.

I would like to take this opportunity to thank all my supervisors for their advice. Furthermore, I want to thank Moog and the staff of the robotics department for their support, without Moog it would not have been possible to realize a complete prototype.

Finally, I would like thank my family, and especially Ilona, for their support.

Dyon Bode

Zegveld, February 2012

Abstract

Tremor, characterized by involuntary and rhythmical movements, is the most common movement disorder. Tremors can have peripheral and central oscillatory components which properly assessed and separated may improve diagnostics. An MR-safe haptic wrist manipulator enables simultaneous measurement of proprioceptive reflexes (peripheral components) and brain activations (central components) through fMRI. For such a MR-safe manipulator, this study determined the design criteria, created the design and presented its prototype.

The prototype is divided into an MR-safe and MR-unsafe part. The hydraulic MR-safe vane motor (end effector) and optical sensors in the MR-environment are connected to the MR-unsafe part in the control room via hydraulic tubes and optical fibers. As a result, the fMRI quality is ensured and the manipulator is suited for safe use in any MR-environment. During a test in an MR-scanner (AMC, Amsterdam) no distortions in the MR-image or sensor signal were observed. The vane motor has a range of motion from -67° to 67° (134° total) with a designed torque delivery of 8 Nm at a 3 bar pressure difference. The achieved accuracy for the torque sensor is $\pm 2\%$ full scale (F.S. = 14.3 Nm) and for the absolute position sensor $\pm 1\%$ full scale (F.S. = 70°=1.22 rad). The measurement range for the position sensor was 70°, however with an adjusted encoder disc this can be increased to match the vane motor's range of 134°. The prototype vane motor had some leakage along the axis, this prevented the use of pre-pressure and consequently reduced the bandwidth and maximum torque. However the maximum achieved torque of 1.5 Nm was still enough to met the requirement of 1.2 Nm. A PI controller was used to control the system, however this controller could not cope with the inherent non-linearities of hydraulics over the intended bandwidth (20 Hz). During the tuning of the PI controller good position tracking results were obtained for 1 and 2 Hz sine commanded motions, which showed no signs of stick-slip effects. Despite the fact that the controller was not optimal, typical responses were obtained with impedance FRFs of two inertial loads.

For future research it is recommended to remedy the axis leakage and implement a model-based controller. The open-loop FRF of the commanded velocity to the measured vane velocity was determined to characterize the system. Even with leakage and without pre-pressure, the measured bandwidth (-3 dB or $\sqrt{0.5} \approx 0.707$ gain) was approximately 5 Hz and the -180 $^\circ$ phase is passed at 7 Hz. Although the bandwidth does not fulfill the requirement for proprioceptive reflex identification it does allow for various motor control experiments. With the recommendations carried out, it is expected that the next prototype will be suited for proprioceptive reflex identification during fMRI

Contents

1 Introduction

1.1 Motivation

Movement disorders severely impair a person's ability to produce and control bodily movements. In 2005, a population-based study showed that for a total of 706 men and women aged 50-89 years, the prevalence of all common categories of movement disorders was 28%, with tremor being the most common category (14.5% prevalence). Moderate-to-severe disease expression was found by half of all patients, however standard drug treatment was only given to 7% (Wenning et al., 2005). The study concluded that there is a high prevalence of, and substantial under-recognition and under-treatment of movement disorders in the general community. Tremor is the most common movement disorder and characterised by the involuntary, rhythmical movement of a body part (Deuschl et al., 1998). The body parts affected by tremor are: arms, head, trunk and legs. However most tremors occur in the hands (NINDS, 2006).

Motor control is regulated by the central nervous system (CNS), comprised of the brain and spinal cord. Figure 1.1 shows an overview of neural motor pathways. The spinal cord transports the motor commands from the brain to the spinal motorneurons. The peripheral nervous system (PNS) transports the motor commands and sensory feedback respectively from and to the CNS. Peripheral reflexes are fast involuntary movements in response to sensory feedback. When the frequency of the tremor depends upon the inertial and elastic properties of the limb and its load, then it has at least in part, a mechanical reflex component, which means that the tremor is produced by the oscillations in peripheral feedback loops. When the frequency of the tremor is not influenced by stiffness and inertia modifications and independent of the peripheral feedback loop properties, then it is a central neurogenic tremor and believed to originate from an oscillating neural network within the brain (Elble, 1996). A tremor can thus have two oscillatory components, a peripheral reflex component and a central neurogenic component (Grimaldi and Manto, 2008).

Several types of tremor exist, i.e. essential tremor (Louis and Vonsattel, 2008), Parkinsonian tremor (Jankovic, 2008) and intention tremor (Deuschl et al., 2000). For these disorders it is known that they have a central neurogenic component (Elble and Deuschl, 2002). Early and precise diagnosis of tremor is crucial for the correct and thus most effective treatment, however currently the clinical diagnosis of tremor is limited, subjective and fails to include the peripheral and central oscillatory components.

Both oscillatory components can be analyzed. The analysis of the central neurogenic component uses functional Magnetic Resonance Imaging (fMRI), which is a specialized type of Magnetic Resonance Imaging (MRI): a non-invasive imaging technique that uses strong magnetic fields and radio frequency pulses to visualize the internal human body. With fMRI, the location of oxygen consumption related to brain activity can be visualized during motor tasks. With the use of a haptic manipulator the peripheral reflex component can be analyzed. A haptic or force-controlled manipulator allows for unambiguous motor tasks and application of continuous random force perturbations. Such perturbations feel natural to the subject and evoke the use of proprioceptive reflexes. The haptic manipulator can than measure the response of the subject to the perturbations to identify the joint's endpoint admittance: the causal, dynamic relationship between a force (input)

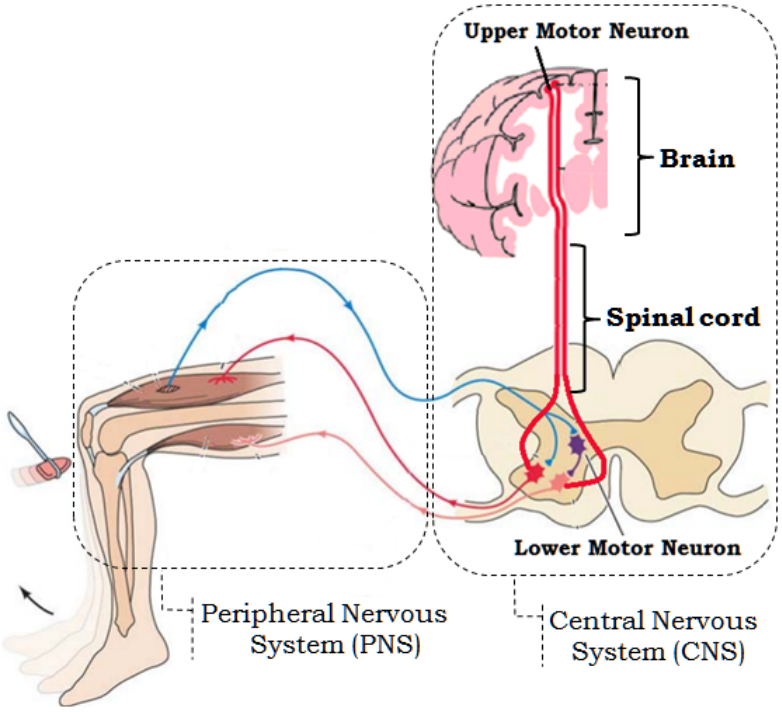

Figure 1.1: Simple schematic representation of neural motor pathways to illustrate the origins of the peripheral reflex and central neurogenic oscillatory components. Picture adopted from Damjanov (2000) and Kandel et al. (2000)

and position (output). Closed-loop system identification techniques and neuromuscular modelling are then used to quantify the reflexes (Kearney et al., 1997; Mirbagheri et al., 2000; van der Helm et al., 2002; de Vlugt et al., 2002).

Problem statement

The central and peripheral component of tremor can be investigated separately. However since the two components influence each other, the best way to investigate tremor is by measuring both components simultaneously. Simultaneous measurement of the two components would be possible by using a haptic manipulator and MR-scanner at the same time. However since fMRI is sensitive to magnetic disturbances and uses a strong magnetic field, it disallows the use of electrical conductive or magnetic materials in a haptic manipulator. Therefore, the haptic manipulator must be MR-compatible. The problem is that currently it is not possible to simultaneously analyze the peripheral and central oscillatory components of tremor. Since current MR-compatible haptic manipulators do not comply with the requirements needed for proprioceptive reflex identification.

Goal

The goal was to design a haptic wrist manipulator suited for safe use in any MR-environment and capable of proprioceptive reflex identification during fMRI without comprising image quality.

2 Background

A haptic (wrist) manipulator needs an actuator, torque sensor and position sensor. In Figure 2.1 a simple schematic representation is given of a haptic wrist manipulator. The subject interacts with the actuator through a handle, which contains a torque sensor so that the interaction torque can be measured. The position of the handle is also measured and together with the torque fed back to the control computer for the determination of the correct actuation.

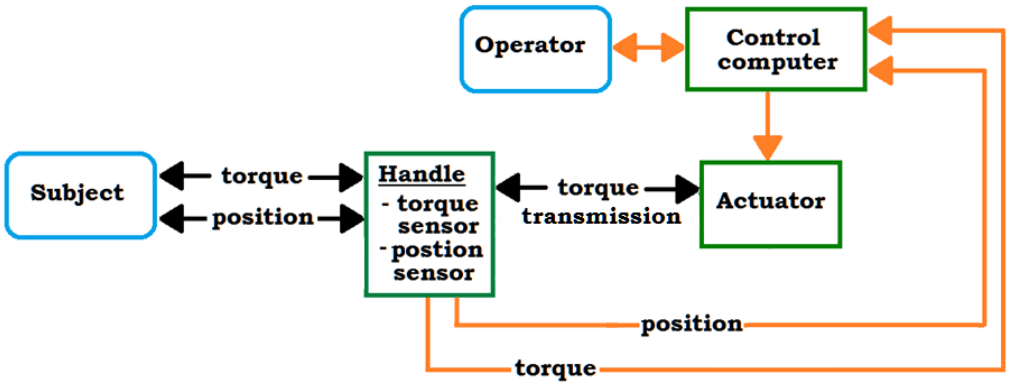

Figure 2.1: Simple schematic representation of the components in a haptic wrist manipulator. The orange lines indicate signals containing information or a command. The black lines indicate physical interactions, i.e. transfer of a position or torque.

2.1 Requirements

As a requirement the manipulator must be suited for safe use in any MR-environment and may not deterioration fMRI image quality. The Food and Drug Administration (FDA) recognized American Society for Testing and Materials (ASTM) standard F2503 describes the safety definitions for medical devices in MR-environments. This standard used to describe the terms MR-compatible and MR-safe, however the term MR-compatible was often misinterpreted and incorrectly used (Schaefers, 2008). Therefore, in 2005 the ASTM revised the standard F2503 and no longer uses the term MR-compatible, instead only the official terms MR-safe, MR-conditional and MR-unsafe are used (ASTM, 2008; Kanal et al., 2007; Gassert et al., 2008a). Nonetheless, in literature the term MR-compatible is still often used to indicated that the use or design of a device is meant for in an MR-environment. However, only the official terms as described in ASTM F2503 will have any value regarding MR-safety. An item that has been demonstrated to pose no known hazards in a specified MR environment with specified conditions of use is MR-conditional. A device is deemed MR-safe when it poses no known hazards in any MR-environment. In practice, MR-safe means that the manipulator is constructed from electrical non-conductive and magnetically compatible materials, such as plastics, glass and rubber.

Furthermore, the use of these materials does not require MR-compatibility testing in every new MR-environment. Therefore it is the requirement to make the manipulator MR-safe instead of just MR-conditional. This ensures fMRI quality and makes it suited for safe use in any MR-environment, i.e. independent of an unique facility or MR-scanner features. From a user and commercial perspective, avoiding any risk and thereby discussion is a great advantage of MR-safe equipment over MR-conditional equipment. Besides the MR-compatibility requirements there are several functional requirements.

Degrees of freedom
Flexion and extension of the wrist is the motion of interest for the wrist manipulator. It is a common choice in wrist manipulator design to have 1 rotating DOF to allow flexion/extension and exclude ab- and adduction of the wrist to simplify the design (Schouten et al., 2006; Gassert et al., 2006). A $\pm 40^{\circ}$ range of motion is sufficient to allow functional flexion and extension movement of the wrist joint.

Bandwidth
To study the neuromuscular response, the haptic manipulator needs to be fast, smooth and needs to have sufficient perturbation bandwidth to test the subjects over the entire frequency range with relevant dynamics (de Vlugt et al., 2003). Smooth means that the movement does not consist of discrete steps. The eigenfrequency of a (co-)contracted human wrist is approximately 15 Hz (Schouten et al., 2006) and according to Perreault et al. (2001) all dynamics of a human arm are excited under 20 Hz. Therefore the bandwidth of the haptic wrist manipulator should be at least 20 Hz (Gassert et al., 2006).

Inertia and friction
The amount of inertia and friction after the torque sensor needs to be minimal because the controller cannot compensate for that. If the inertia and friction are negligible it will feel for the subjects as if they are moving freely. To accomplish this effect Williams (2001) quantified that the perceived values of the inertia and friction by the subjects need to be respectively between 2.9 and 4.3 g m^2 and 0.21 Nm at maximum. For a human wrist 3 g m^2 is an average value for rotational inertia about the flexion and extension axis (Williams, 2001). Another study with a haptic wrist manipulator achieved an perceived endpoint inertia of 1.6 g m^2 and found an average value for the wrist inertia of 1.42 g m^2 (Schouten et al., 2006). The difference between values found for the rotational inertia was contributed to the fact that with the use of the manipulator the hand was closed, i.e. flexed fingers and in other anthropometric data sources the hand is often open, i.e. extended, slightly bent fingers. For the MR-safe manipulator the perceived inertia and dynamic friction should be respectively 4.3 g m^2 and 0.21 Nm maximal.

Size and portability
The dimensions of the haptic wrist manipulator are limited by the space available around a patient inside a closed bore MR-scanner. A closed bore MR-scanner is typically 60 cm in diameter and 1.5 to 2 m long (Tsekos et al., 2005). The space available around a 1.85 m tall person weighing 100 kg in an MR-scanner bore (60 cm diameter and 160 cm length) is between 8-12 cm next to, and 12-15 cm above the person (Christoforou et al., 2006). The system must be independent of the MR-setup, i.e. not be dependent on unique facility or MR-scanner features. The average dimensions of a wrist and hand lead to a handle length of 110 mm with a diameter of 32 mm. The distance between the wrist axis and the handle is on average 70 mm and needs to be adjustable so that the wrist axis and rotational axis of the haptic manipulator can be aligned (Schouten et al., 2006). The forearm needs to be clamped to isolate movement of the wrist (Tsekos et al., 2005; Christoforou et al., 2006).

Torque
The delivered torque must be adequate to perturb a wrist. For flexion and extension the minimal required torque is 1.2 Nm, since that is sufficient to accelerate the wrist and perturb a contracted wrist (Williams, 2001). However if it would be possible to achieve torques in the range of 6-10 Nm the manipulator would also be able to perturb a fully co-contracted wrists, nevertheless 1.2 Nm is the requirement (Grimaldi et al., 2008; Schouten et al., 2006).

Safety
The manipulator should pose no hazard risk, be MR-safe and have a physical limitation to the range of motion. An emergency button which stops the haptic manipulator should be present and patients should be able to quickly release the forearm.

Cost effectiveness
Functionality weighs heavier than cost. In the case of multiple solutions which comply with the requirements, the one with the lowest cost for series production is preferable.

Summary list of requirements

The requirements are summarized into two sections, the first section are requirements that are strict and have to be met. The second section are requirements with preferred values for the different properties that should be met as close as possible to the desired values but can be compromised on, e.g. a bandwidth less than 20 Hz. The second section is in order of importance, starting with the most important.

Strict requirements:

- The device should pose no hazard risks, be MR-safe, not cause image artifacts or deteriorate fMRI image quality and have an emergency stop button.
- A 1 DOF for wrist flexion and extension with physical limitation to range of motion.
- The dimension must allows use in an MR-scanner bore of 60 cm in diameter. The width space available next to a person is approximately 120 mm.
- The device should be able to comfortably and safely clamp the forearm
- Fast and smooth motion with a torque delivery of at least 1.2 Nm

Preferred requirements:

- The bandwidth should be at least 20Hz.
- A range of motion of $\pm 40^{\circ}$ from the initial position.
- Inertia and dynamic friction should be respectively 4.3 g m^2 and 0.21 Nm maximal.
- The system must be independent of the MR-setup, i.e. not be dependent on unique facility or MR-scanner features.
- With similar performance, the most cost effective solution is preferred.

2.2 Actuation solution

Conventional electromagnetic motors cannot be used in an MR-environment (Burdet et al., 2006). There are alternative electric based actuators used in MR-compatible systems, e.g. electrostatic actuators (Yamamoto et al., 2005), electrorheological fluid actuators (Khanicheh et al., 2006), and piezoelectric motors. Piezo motors are often used when the robot is mostly stationary and actuation is needed to move the robot into another stationary position (Tsekos et al., 2008; Chinzei et al., 1999; Elhawary et al., 2008; Flueckiger et al., 2005). The advantages of a piezoelectric motor are that it does not require, or is affected by a magnetic field and it delivers a high torque at low speed, has high responsiveness, controllability and is compact. However these alternatives are not suited, since they still use an electric field which can deteriorate fMRI quality and are not MR-safe due to the use of conducting materials.

Due to the limited space available in the bore of an MR-scanner or due to MR incompatibility, actuation solutions are often used in combination with a transmission such that the actuator can be placed outside the bore or even the MR-environment. This has the advantages that larger actuators can be used and image artifacts caused by the actuator are prevented. The disadvantage is that the typical distance from control room to MR-scanner bore 9 m is and that a transmission will introduce friction, backlash, elasticity and time delays depending on the type of transmission (Tsekos et al., 2008; Christoforou et al., 2006; Yu et al., 2008). The transmission of the force or torque created by an actuator can be achieved with a belt, linkage or shaft system. These systems are not suited as an actuation solution since they have facility-specific designs and therefore lack flexibility, thus failing to comply with the requirement of independence on an unique facility or MR-scanner features. Several remaining actuation solutions were assessed using the requirements.

Hydraulic or pneumatic valve system
An actuation solution that uses hydraulics or pneumatics piston-cylinders constructed out of MR-compatible materials has the advantage that is inherently MR-safe. When the hydraulic tubes are made long enough to reach the control room of an MR-scanner, easily controllable conventional electromagnetic motors pose no problem as a pressure source. However results from studies (Yu et al., 2008) that use these systems with long tubes do not achieve a sufficient bandwidth to comply with the requirement for the manipulator.

Pneumatic step motor
For the development of the MrBot robot a new MR-safe new pneumatic step motor was designed called the PneuStep (Stoianovici et al., 2007). The PneuStep achieves its discrete rotary motion by sequentially pressuring three ports and is MR-safe by using only non-magnetic and dielectric materials such as ceramics, rubbers and plastics. The PneuStep has its own integrated gearhead and optical incremental position encoder, making the actuator electricity free and only using compressed air and light. However the stepping nature and the amount of torque that can be delivered fail to comply with the smooth movement and torque requirements, making the PneuStep not a suitable actuation solution for the haptic manipulator.

Bowden cables
A Bowden cable consist of an outer cable housing with an inner cable transferring mechanical force. They are mostly used to deliver a pull force but can also deliver a small push force over a short distance. The weight-to-length ratio of these cables is low which

means that the movement inertia is limited and the transmission is linear. A study done by Chapuis et al. (2006) used a cable transmission system which is comparable with a system of two Bowden cables. However, Bowden cables would have more friction which opposes smooth motion. The study showed a bandwidth of about 30 Hz over a distance of 9 m. However Bowden cables are made of steel which could lead to image distortions. If at all possible, making the cable out of a MR-compatible material results in an insufficient bandwidth due to the lesser mechanical properties compared to steel. In conclusion, the Bowden cables solutions is not suited for the haptic manipulator.

Hydraulic master-slave system
The advantages of the hydraulic or pneumatic valve system actuation solution apply to the hydraulic master-slave solution. However instead of using valves, this solution uses a master and slave piston-cylinder with pre-pressurized transmission tubes in a closed circuit. With a tube length of 10 m the achieved bandwidth was 20 Hz and there was no deterioration of fMRI image quality (Gassert et al., 2006).

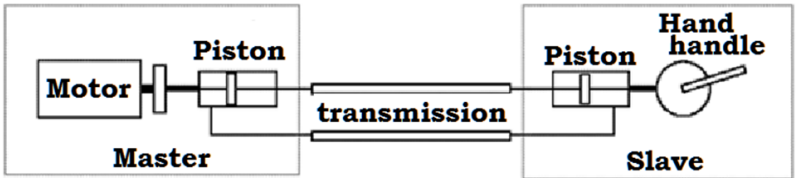

Figure 2.2: Schematic representation of the hydraulic master-slave system. Adopted from Gassert et al. (2006)

Conclusion
The requirements regarding MR-safety & fMRI quality, force-perturbation bandwidth, smooth motion and torque are the most important with respect to the actuation. An overview of is given in Table 2.1.

Requirement: / Solution:	MR-safe & fMRI quality	Bandwidth	Smooth motion	Torque
Hydraulic master-slave system	+	+	+	+
Hydraulic / pneumatic valve systems	+	-	+	+
Pneustep (pneumatic step motor)	+	-	-	-
Bowden cables	-	-	-	+

Table 2.1: Actuation solutions assessed against the applicable requirements. A + sign indicates that the solution complies with the requirement, the - sign indicates that it failed to comply.

As mentioned before and clear from Table 2.1, the hydraulic master-slave actuation solution is best suited as it complies with all requirements. This solution is used as an basis for the design of the actuator.

2.3 Sensing solution

Conventional strain gauges, commercial torque sensors and position sensors have non-MR-compatible electronic and material parts and thus, due the MR-compatibility constraints, cannot be used. Others have used electrically active sensors constructed out of MR-compatible materials. Electrically active sensors have electronic components inside the MR-environment. With the proper precautions, i.e. shielding and a sufficient distance from the imaging area, the amount of image artefacts and noise can be acceptable (Khanicheh et al., 2006; Hidler et al., 2005). However this means that the sensor needs to be tested for every different imaging sequence or MR-scanner to see if it is still usable. This is very demanding, time consuming and future new sequence and MR-scanners cannot be anticipated. To prevent any electromagnetic interference and ensure the sensors compatibility for any imaging sequence, it is best to use a sensor without an electrical component and wiring inside the MR-room. This means that the sensor information needs to be transported outside the MR-environment, and that the material and medium used for this transport are MR-safe and isolate the electrical components at the end from the MR-room. This can for instance be accomplished by transferring the measurement information inside the MR-environment, with fiber optic cables, to outside the MR-environment where the use of conventional electronic equipment is not a problem.

Hydraulic sensor
A hydraulic force sensor can be used during fMRI without compromising image quality (Liu et al., 2000). The handle and cylinder are the only parts of the sensor in the MR-environment and thus made out of MR-safe materials. Via a tube, the fluid pressure in the cylinder is transferred out the MR-environment to the electronic pressure sensor and amplifier in the control room. The sensor was calibrated and proved to provide a linear relationship between force and transducer output voltage. However due to friction the linear relation is only true beyond a certain force level (50N). This sensor principle is not suited for the MR-safe manipulator because the hydraulic transmission makes it impossible to achieve the necessary high measurement frequency for haptic robot control.

Fiber optic light intensity measurement sensors
Fiber optics provide a transmission of signals which is MR-compatible, have simple and flexible installation and negligible signal loss or time delays over long distances. Light intensity measurement sensors use an emitting and receiving fiber, making binary encoder sensors for translation and rotation or simple on-off switch possible (Gassert et al., 2006). Furthermore force or torque sensors can be constructed with this principle by applying the receiving and emitting fibers on to a deformable body. When the body is deformed, as the result of an applied torque or force, the reflected light intensity changes and can be measured (Chapuis et al., 2004; Yu et al., 2007, 2008; Flueckiger et al., 2005; Masayuki et al., 2009).

Conclusion
Most applicable for the sensor solutions are the requirements regarding MR-safety & fMRI quality and the force-perturbation bandwidth, thus the sample rate of the sensor. The principle must also be suited to create a position and torque sensor. An overview of the two sensor solutions against the just mentioned requirements is given in Table 2.2. The fiber optic light intensity measurement principle complies with all the requirements and is ideally suited to create torque sensors and rotational encoders.

Requirement / Solution	MR-safe & fMRI quality	Bandwidth	Position sensor	Torque sensor
Hydraulic sensor	+	-	-	+
Fibre optic light intensity measurement sensors	+	+	+	+

Table 2.2: Sensor solutions assessed against the applicable requirements. A + sign indicates that the solution complies with the requirement, the - sign indicates that it failed to comply.

3 Design

Forming a design for a haptic manipulator according to the requirements and based on best suited design solutions required MR-safe position and torque sensors and a MR-safe hydraulic vane motor. However these parts were not commercially available and needed to be designed and custom-made.

3.1 Actuator: hydraulic vanemotor

The actuator is based on the closed circuit hydraulic master-slave actuation solution. However instead of using a cylinder-piston configuration a vane motor in combination with a hydraulic pump is used. The vane motor acts as the slave and the hydraulic pump as the master. A vane motor is a fluid (hydraulic or pneumatic) powered actuator that converts a fluid pressure or flow into a angular displacement and torque. The stator and rotor are the two main parts of a vane motor.

The first of the two main advantages of the modifications to the hydraulic master-slave solution, is that a vane motor directly gives a rotational motion, where as a cylinder-piston configuration gives a linear movement. This linear motion needs to be converted in a rotation which requires additional equipment, making the vane motor a more compact and less complex choice. The second main advantage is that a vane motor allows for leakage across the rotor. If there was any leakage in the piston-cylinder configuration the master and slave piston would go out of sync, since the master side cannot compensated this. This is not a problem with a vane motor as the hydraulic pump has no constraints with regards to pumping fluids in either direction.

In the design of a vane motor the choice has to be made whether to allow leakage or not. Since leakage is not a problem and creating a completely leakage free vane motor is almost impossible without strenuous sealing and thus considerable friction, the choice is to design a vane motor that is allowed to have some leakage around the rotor. This has the advantages that the vane motor will have a certain degree of backdriveability, damping and the design is less difficult because there is no addition sealing needed between the rotor and stator. Less seals also means less friction which is another advantages as it promotes smooth motion. The disadvantages of leakage are that a larger pump discharge is needed and that the position of the hydraulic master pump does not correspond with the position of the rotor in the vane motor, thus requiring a position sensor on the rotor. However a position sensor was already needed for the control of the haptic manipulator.

A schematic representation of the complete actuation solution is presented in Figure 3.1. Besides the vane motor and hydraulic pump the third part of the actuation is an electro motor that drives the hydraulic pump. Which is another advantages with respect to the piston-cylinder configuration, since the translation of the piston requires a linear motor instead of a more convenient conventional rotational electro motor.

Since the required range of motion is less than 180°, a vane motor with a double vane can be used. This has the advantage that the axis of the rotor experiences a couple or pure moment instead of a moment which would be the case with a single vane. Compared to a single vane, the use of two vanes results in less deformation of the rotor axis and less friction between stator and rotor. Furthermore a couple provides twice the torque, given the same actuator dimensions. The disadvantage of two vanes is that the design is more complex since the fluid has to reach the vanes on opposite sides of the rotor axis.

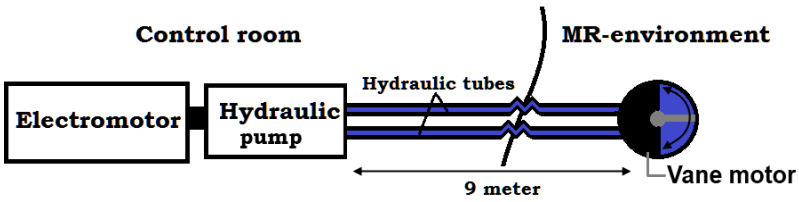

Figure 3.1: Schematic representation of the hydraulic master-slave actuation system. The vane motor acts as the slave in the MR-environment and the hydraulic pump, driven by an electro motor, acts as the master in the control room

This means that at least one set of supply ducts intersect and need to cross each other. Figure 3.2 illustrates theses crossed ducts. The outer diameter of the vane motor is 120 mm, which is determined to be the maximum space available besides a person inside an MR-scanner bore (Tsekos et al., 2005; Christoforou et al., 2006).

The diameter of the vane is as large as possible so that the moment arm to the rotor axis is as well. This means that the required force, and thus pressure, can be as low possible to meet the the torque requirement. A lower pressure is beneficial with regards to leakage, safety and deformation of the vane motor. As a result of the maximized moment arm, the required area of the vanes is such that the diameter of the rotor axis can be increased to reduce the chamber volume (Figure 3.2a). This had the advantage that for the same translation of the vane, the flux of oil can be reduced and with it the inertia effects of the moving oil. Even though the larger rotor diameter reduces the effective vane area, the vane motor is capable of delivering 8 Nm of torque at a 3 bar pressure difference and has a range of motion from $-67°$ to $67°$ ($134°$ total).

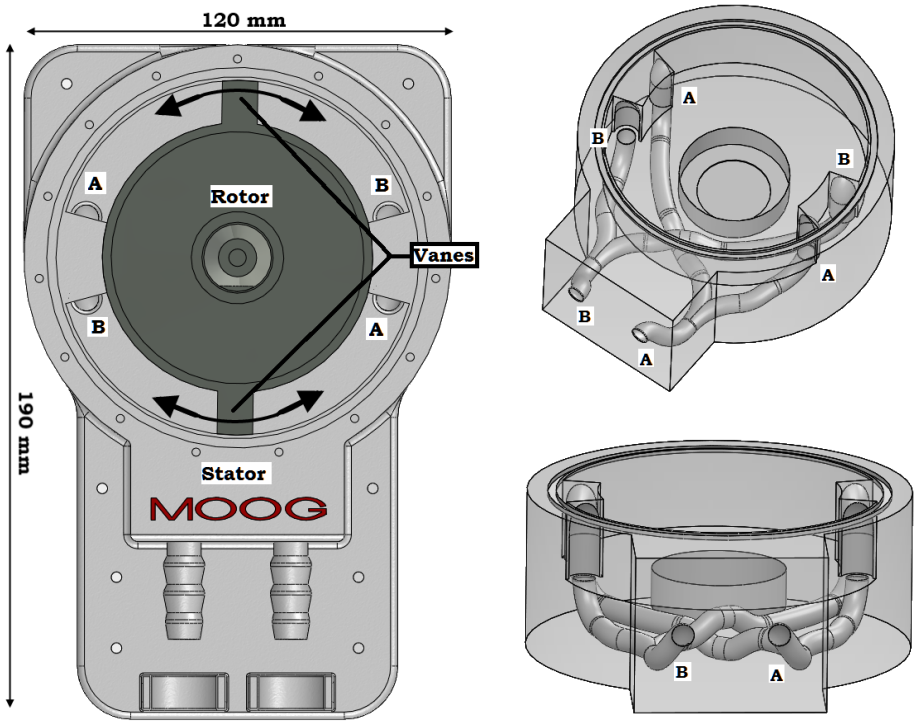

(a) (b)

Figure 3.2: Drawings of the vane motor. Coupled cross-linked fluid in/outlets are labeled either A or B. (a):Top view drawing of the vane motor with cover removed. (b):Transparent drawing of the base stator illustrating the cross-linked fluid ducts.

3.2 Sensors: light intensity measurement

As concluded the best suited solution to create MR-safe sensors is by applying the fiber optic light intensity principle. There are two methods to apply the light intensity principle to measure displacement, using *opposing fibers* or a *reflective surface*. The advantage of using a reflective surface is that the emitting and receiving fiber are one the same side of the sensor and can be located in one sensor head. Having the fibers in one sensor head also prevents the need to align the emitting and receiving fiber which would be necessary using opposing fibers.

Using a *reflective surface* two methods, the *distance* and *knife-edge* method are available. The *distance* method provides increased sensitivity because the distance travelled by the reflective surface, is double the distance on the receiving fiber. However the *knife-edge* method gives a more definitive and clearer signal and will be used in the position and torque sensor. Figure 3.3 shows the two reflective surface methods.

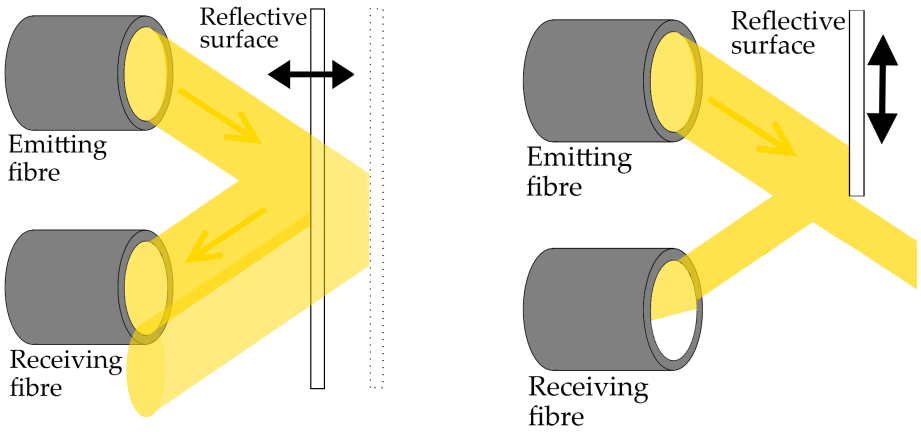

(a) Reflective light intensity *distance* method.

(b) Reflective light intensity *knife-edge* method.

Figure 3.3: Schematic representation of the two *reflective surface* methods.

3.2.1 Torque sensor

The designed torque sensor consists of an optical sensor and a deformable body and is based on the design of a fellow student (Vlaar, 2011). Design changes were made to the optical sensor alignment and handle adjustment components and the dimensions were changed to increase the measurement range to ± 8 Nm. The deformation of the sensor body is detected using the knife-edge method. The used sensor head (Keyence FU-38) is made out of plastics and has receiving and emitting optical fibers of 5 meter, which are connected to the amplifier (Keyence FS-N11MN). The slot for the handle in the sensor body allows the precise alignment of the wrist joint with the axis of the actuator.

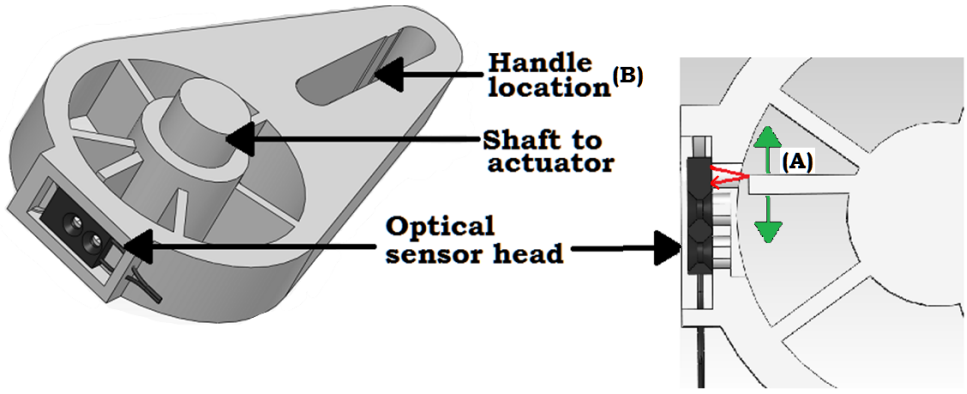

Figure 3.4: Drawing of the torque sensor using the knife-edge method to detect the displacement of (A) with regards to the sensor head when a force is applied to (B). The right part of the drawing is a partial top view.

3.2.2 Position sensor

The position sensor uses a plastic sensor head (Keyence FU-37) also connected to an amplifier (Keyence FS-N11MN) with optical fiber. A disc with an eccentric hole is placed on the axis of the vane motor and acts as an encoder disc. The rotation of the axis changes the amount of reflective surface and thus acts as a unique reference for each position, resulting in a absolute position sensor. Figure 3.5 shows the two extreme configurations of minimal and maximal surface reflection from the encoder disc in respectively Figure 3.5a and Figure 3.5b.

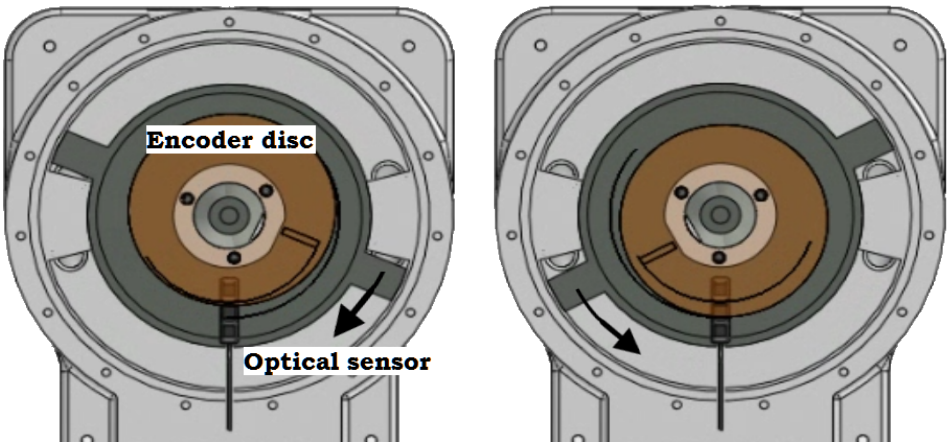

(a) (b)

Figure 3.5: Top view drawings of the absolute optical position sensor. In this rendering the encoder disc is made transparent so that the optical sensor can be seen and extra lines at the edge of the disc are added to indicate the trajectory. (a):the position sensor in one endpoint resulting in the minimal amount of reflective surface from the encoder disc. (b): the other end point position resulting in the maximal reflective surface from the encoder disc.

3.3 Complete system prototype

The parts for the prototype of the MR-safe haptic wrist manipulator are manufactured out of three materials and fabricated using the rapid prototype techniques stereolithography and selective laser sintering (Materialise, Leuven, Belgium). Rapid prototype techniques were used for the construction of the prototype because of the high level of design freedom, inherent MR-safe plastic materials and most importantly a short realization time. The high level of design freedom is also a important advantage because it allowed for the use of internal ducts in the vane motor. With conventional manufacturing techniques this would not have been possible and the connecting hydraulic tubes had to be fitted outside the vane motor and because of the double vane, approaching from two sides. Since the manipulator is used in an MR-scanner bore the space is limited and it would be necessary to fit the external tubes tightly around the vane motor, leading to sharp bends in the tubes and thus more pressure loss compared to the internal ducts. The vane motor stator and rotor as well as the torque sensor are constructed out of the material *Nanotool*™ (DSM Somos ® Nanotool ™). Nanotool was chosen as an material because it has the best mechanical properties of the available rapid prototype materials. And it has an excellent detail resolution, along with superior sidewall quality compared to other stereolithography materials. The cover for the vane motor is made out of the transparent material *TuskXC2700T*, since especially in a prototype it is an advantage to be able to visually inspect (e.g. air pockets, wear) the internals of the vane motor without opening it. The housing and cover for the position sensor are constructed out of polyamide with glass particles. Polyamide was chosen because its properties were sufficient for a sensor housing and it is more than 4 times less expensive than Nanotool.

Table 3.1: Overview of material properties

	Tensile modulus	Tensile strength	Elongation at break
Nanotool	11-11.4 GPa	61.7-78 Mpa	0.23%
TuskXC2700T	2.65-2.88 GPa	47.1-53.6 MPa	11-20%
Polyamide GF	3.8 GPa $\pm$0.15 GPa	51$\pm$3 MPa	6$\pm$3%
Aluminum 6061 T6	69 GPa	310 MPa	17%

The aluminum properties are for reference. Sources: Materialise datasheets and Calister (2003).

Figure 3.6 show a photograph of the complete system prototype, which main parts are the actuator, sensors and real-time computer.The prototype for the actuator is build using a Moog servo drive (G392-008) and electro motor (C-100) with a rated torque and speed of respectively 6 Nm and 3000 rpm. The servo drive operates at update rates of 8 kHz for the velocity and position control loops and 16 kHz for the current control loop. The electro motor is connected to a hydraulic reversible gear pump from Galtech (2SM-A-4-R) with a displacement of 4 cc/rev and an allowed maximum continuous pressure of 230 bar. The 9 meter long tubes connecting the hydraulic pump and vane motor are from Hebu (0503-06). The tubes consist of a synthetic rubber inner ($3/8''$) and outer mantle with 2 woven fabric inlays and is rated for a working and bursting pressure of respectively 110 and 440 bar. As an hydraulic fluid vegetable oil is used because of its non-toxic, non-corrosive nature and easy availability. The real-time computer controls the system and operates at a sample frequency of 2048 Hz and samples the torque and position signals with a 16-bit resolution.

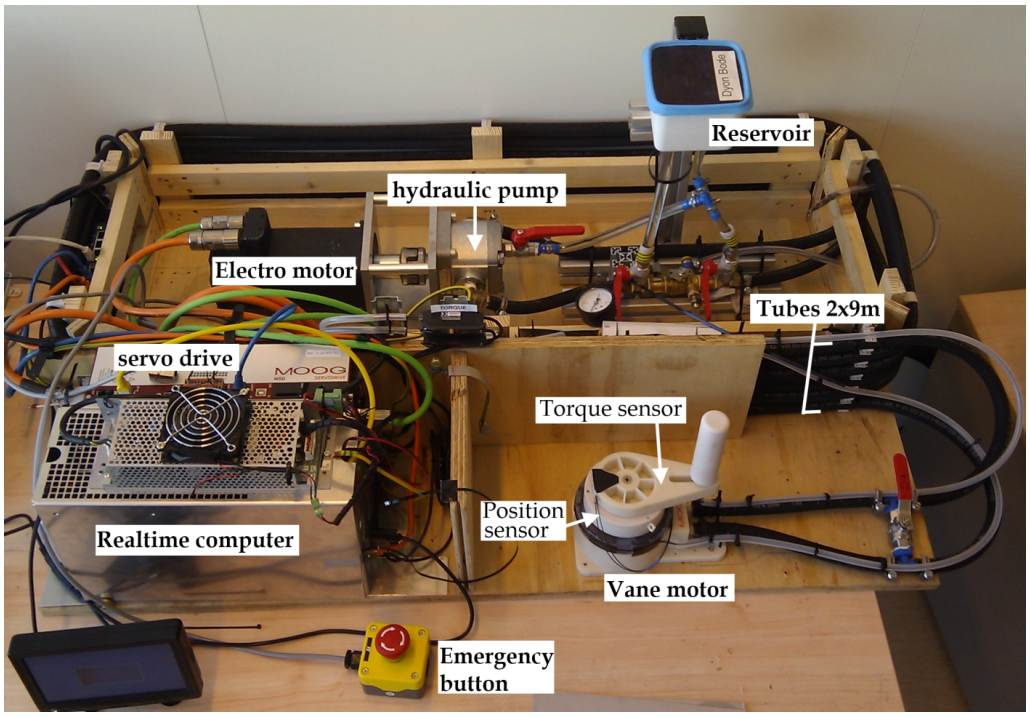

Figure 3.6: Photograph of the complete system prototype. Indicated are the real-time computer, electro motor and drive, hydraulic pump, reservoir and valves, 2 x 9 meter tube, emergency stop button, vane motor and the optical sensors.

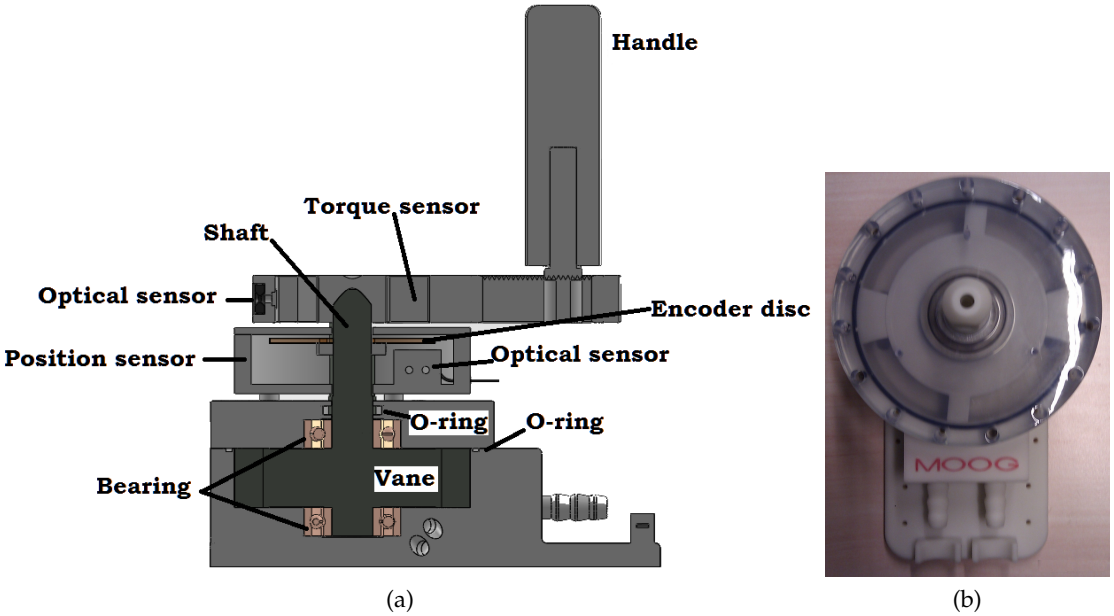

(a) (b)

Figure 3.7: (a): A cross-sectional drawing of the vane motor with torque and position sensor. (b): Top view photograph of the drawing displayed in (a), without the sensors.

3.4 Control

The real-time computer used a virtual model and controls the system with a proportional integral (PI) controller. The Zieger-Nichols method was applied to tune the PI controller by setting K_i to zero and increasing K_p until the ultimate gain K_u at which the output starts to oscillate with period P_u. The gains are than $K_p = 0.45 \cdot K_u$ and $K_i = {}^{1.2 \cdot K_p}/_{P_u}$. However during tuning it became evident that there was not a set of gains to accurately control the system over the desired bandwidth . To improve performance an additional parallel feed forward gain (K_{leak}) to the commanded velocity was implemented to compensate for the internal leak of the vane motor related to the applied torque. Measurements were conducted to determine this relation by applying different static loads to the handle and measuring the expired time for a certain rotational translation. The gain, K_{leak}, was estimated to be 0.3 ${}^{\text{rad}}/_{\text{Nm} \cdot \text{s}}$. In an attempt to further increase the control performance also an additional gain (K_{fric}) related to the direction of motion was added to compensate for the static coulomb friction, which was determined with a spring scale to be 0.14 Nm. Nevertheless these additions did not fully resolve the issues.

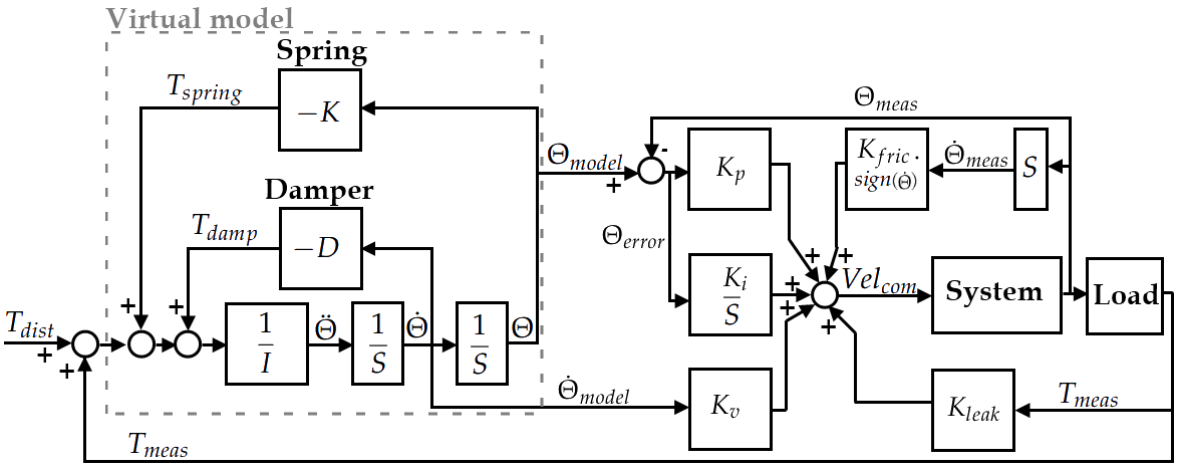

Figure 3.8: Control scheme used in the realtime computer. The system block represents the servo drive, electro motor, hydraulics and vane motor. The measured torque T_{meas} and position Θ_{meas} are measured by the optical MR-safe sensors and are together with the disturbance torque T_{dist} the inputs for the virtual model and controller. During all tests K and D were set to zero, K_v was set to 1 and the feedback of the measured torque T_{meas} to the virtual model was disabled.

4 Verification

To investigate the performance of the MR-safe haptic wrist manipulator prototype several tests were performed to determine the accuracy of the optical sensors and maximum producible torque. During tuning of the PI controller position tracking results for 1 and 2 Hz sine motions were obtained. For the characterization of the system the open-loop frequency response function (FRF) of the commanded velocity to the vane velocity was measured. Finally the impedance FRFs of two inertial loads, i.e. the handle and the handle with a mass, were made. Additionally a test in an MR-scanner (AMC, Amsterdam) was performed which showed no distortions in the MR-image and no distortions in the sensor signal from the manipulator. During all test the feedback of T_{meas} to the virtual model was disabled and the gains for the virtual spring (K) and damper (D) were set to zero and K_v was set to 1.

Optical position sensor
The prototype MR-safe optical position sensor has a measurement range of 70° and was calibrated using a conventional position sensor (Feteris FCP 12AC) with an accuracy of ±1% full scale (F.S. = 300°±5°). After the calibration the measured position of the optical sensor was compared to the measured position of the conventional sensor in a test that was repeated 5 times. The maximum deviation of the position measured with the optical sensor is ±1% full scale (F.S. = 70°=1.22 rad) in relation to the conventional sensor.

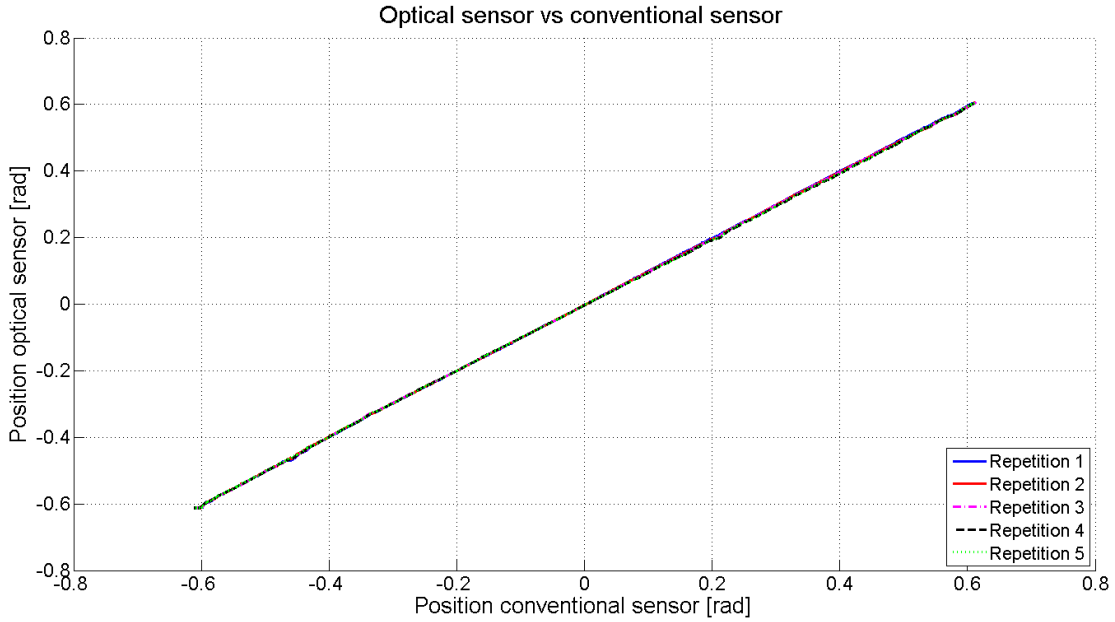

Figure 4.1: Calibration results of the position sensor. Measured position of the conventional sensor against the measured position of the optical sensor

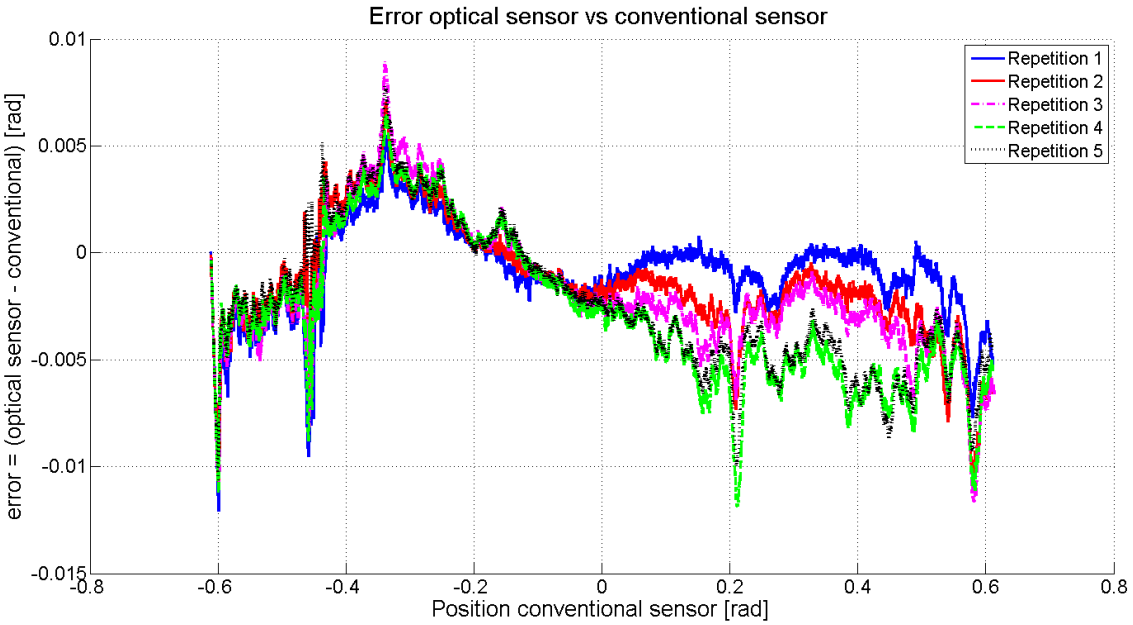

Figure 4.2: Measured position of the conventional sensor against the difference (optical sensor - conventional sensor) between the optical and convention position sensor

Optical torque sensor

The MR-safe optical torque sensor prototype was statically calibrated using a pulley that ensured perpendicular and correct loading of the torque sensor at a moment arm of 91 mm. The calibration test was repeated 4 times and the results showed an accuracy of ±2% full scale (F.S. = 14.3 Nm).

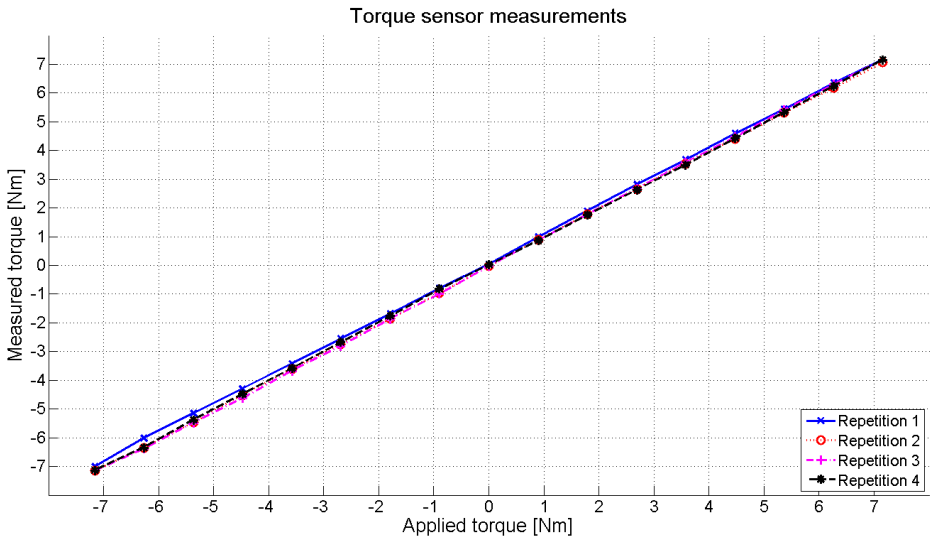

Figure 4.3: Calibration results of the torque sensor. Applied torque against the measured torque by the optical torque sensor

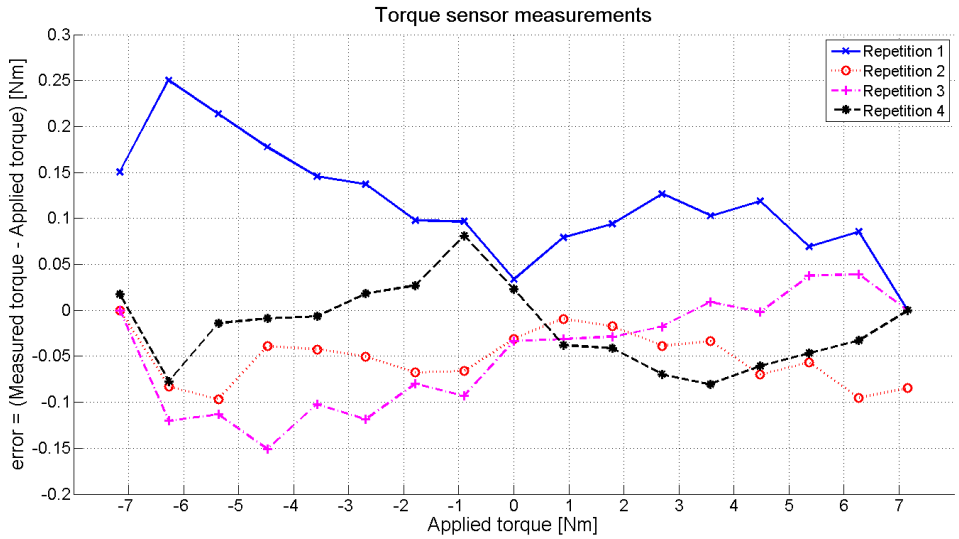

Figure 4.4: Applied torque against the difference (measured torque - applied torque sensor) between the applied and measured torque by the optical torque sensor

Maximum torque
The maximum torque that could be produced with the prototype was determined by fixating the handle to a rigid setup. Several measurements were performed in which the pump velocity was increased until the maximum measured torque was reached, which was 1.5 Nm. During testing cavitation at the inlet side of the hydraulic pump was observed which limited the maximum producible torque.

Open-loop FRF
The electro motor is velocity controlled by its servo controller. To determine the systems characteristics the open-loop FRF of the commanded velocity to the measured vane velocity was determined. The PI controller was not used, i.e. all the gains were zero with the exception of K_v which was set to 1. The commanded velocity input signal was a 30 s flat spectrum multisine with uniformly distributed power between 0.1 and 30 Hz. To exclude transient effects the first and last 7 seconds were removed, leaving a 16 second signal for analysis. The measured signals were sampled at 2048 Hz with a 16 bit resolution. The shown FRF is averaged over 5 measurement repetitions and to improve the estimates, the spectral densities were averaged over 4 frequency bands. The open-loop bandwidth (-3 dB or $\sqrt{0.5}$ ≈0.707 gain) is approximately 5 Hz and at 7 Hz the phase passes -180 °. The open-loop FRF ($\hat{H}_{ol}$) and coherence ($\hat{\gamma}^2_{ol}$) were calculated using spectral densities estimates $\hat{S}(f)$ of input (i) and output (o):

$$\hat{H}_{ol} = \frac{\hat{S}_{io}(f)}{\hat{S}_{ii}(f)} \qquad \hat{\gamma}^2_{ol}(f) = \frac{|\hat{S}_{io}(f)|^2}{\hat{S}_{ii}(f)\,\hat{S}_{oo}(f)} \tag{4.1}$$

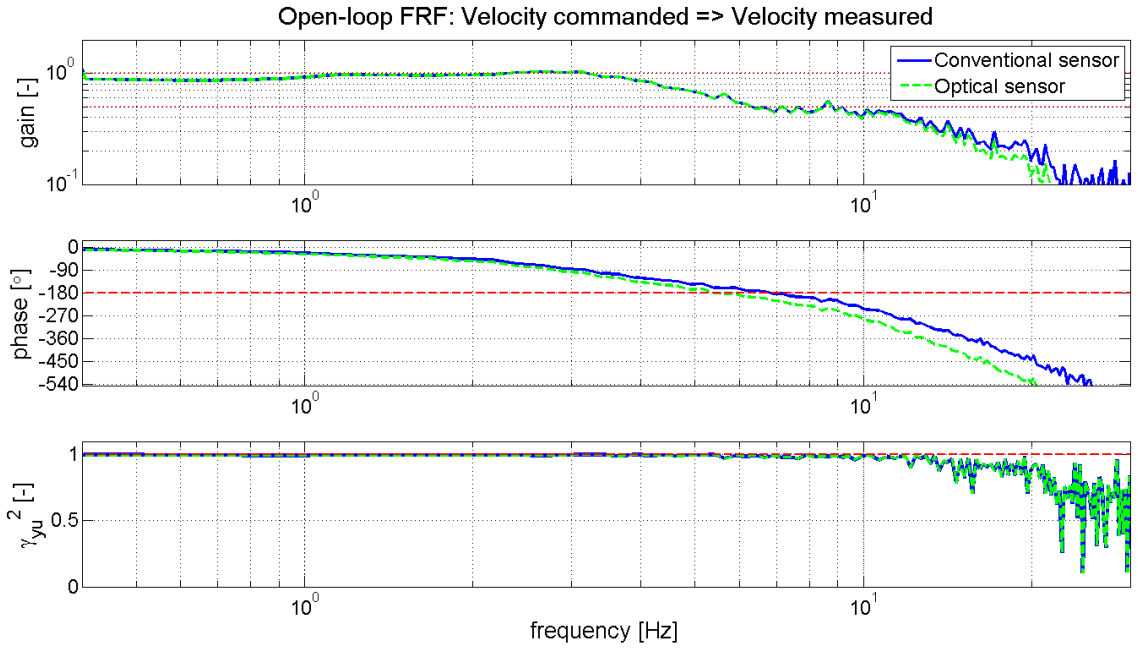

Figure 4.5: The open-loop FRFs of the commanded velocity to the measured vane velocity. For comparison, one FRF is determined with the measurements from the optical sensor, the other with use of the conventional sensor. These FRFs are averaged over 4 repetitions and to improve the estimates, the spectral densities were averaged over 4 frequency bands. The FRF made with the measurements from the optical sensor has an increased phase lag caused by filtering of that measured signal

Position tracking
During the tuning of the PI controller position tracking results were obtained for an 1 Hz and 2 Hz sine (Figure 4.6). The controller settings were different and optimized for the specific 1 or 2 Hz commanded sine position signal, respectively being $K_p = 30$, $K_i = 40$ and $K_p = 25$, $K_i = 15$

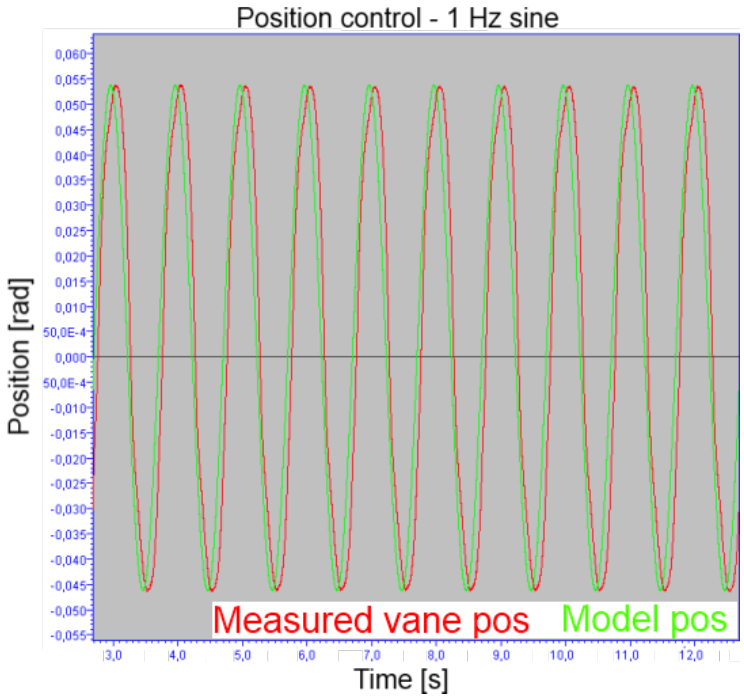

(a)

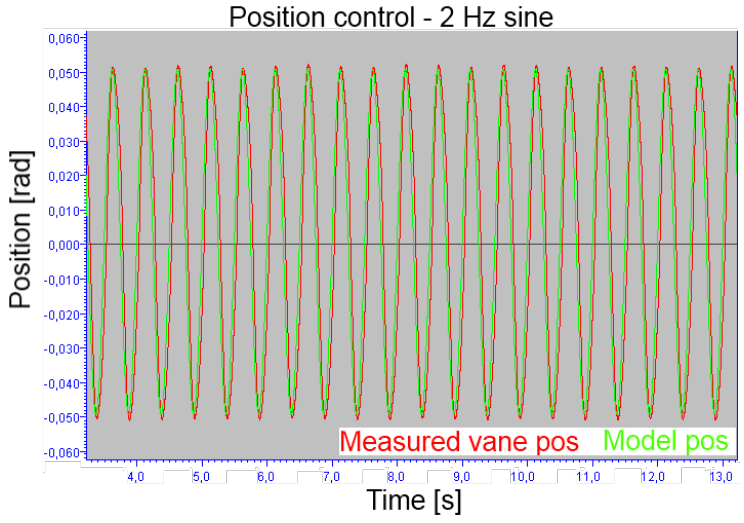

(b)

Figure 4.6: Position tracking results for an 1 Hz (a) and 2 Hz (b) sine obtained during tuning of the PI controller. Different controller settings and optimized for the specific 1 or 2 Hz commanded sine signal were used.

Impedance FRF

Although the controller was not able to precisely control the output position, two load FRFs were determined with only $K_p = 10$, $K_i = 20$ and $K_v = 1$ set. A position disturbance was commanded and the resulting position and torque were measured to determine the impedance for two inertial loads: 1.46 g m^2 (handle inertia) and 3.93 g m^2 (handle + mass of 480g). The inertias of the handle and load were calculated with the use of a SolidWorks model. For the position disturbance a similar multisine signal as for the open-loop test was used. The load FRFs ($\hat{H}_{load}$) and coherences ($\hat{\gamma}^2$) were calculated using the following spectral densities estimates (Schouten et al., 2006):

$$\begin{aligned} \hat{G}_{DT}(f) &= D(f)^* T(f) & \hat{G}_{D\Theta}(f) &= D(f)^* \Theta(f) \\ \hat{G}_{DD}(f) &= |D(f)|^2 & \hat{G}_{\Theta\Theta}(f) &= |\Theta(f)|^2 \end{aligned} \tag{4.2}$$

$$\hat{H}_{load} = \frac{\hat{G}_{D\Theta}(f)}{\hat{G}_{DT}(f)} \qquad \hat{\gamma}^2(f) = \frac{|\hat{G}_{D\Theta}(f)|^2}{\hat{G}_{DD}(f)\,\hat{G}_{\Theta\Theta}(f)} \tag{4.3}$$

of which $D(f)$, $\Theta(f)$ and $T(f)$ are the Fourier transforms of respectively, the command position, measured position and measured torque signals. The $\hat{G}(f)$ are the estimated spectral densities and the complex conjugate is indicated by an asterisk. As expected with the current controller, the FRFs (Figure 4.7) are rough and the coherence shows that the systems suffers from non-linearities. However a typical second-order response can be seen and the response of the greater inertia is lower with respect to the smaller load as expected. The theoretical FRFs for the load inertia's calculated with SolidWorks are plotted in dashed magenta lines and line up with the trend for the estimated FRFs .

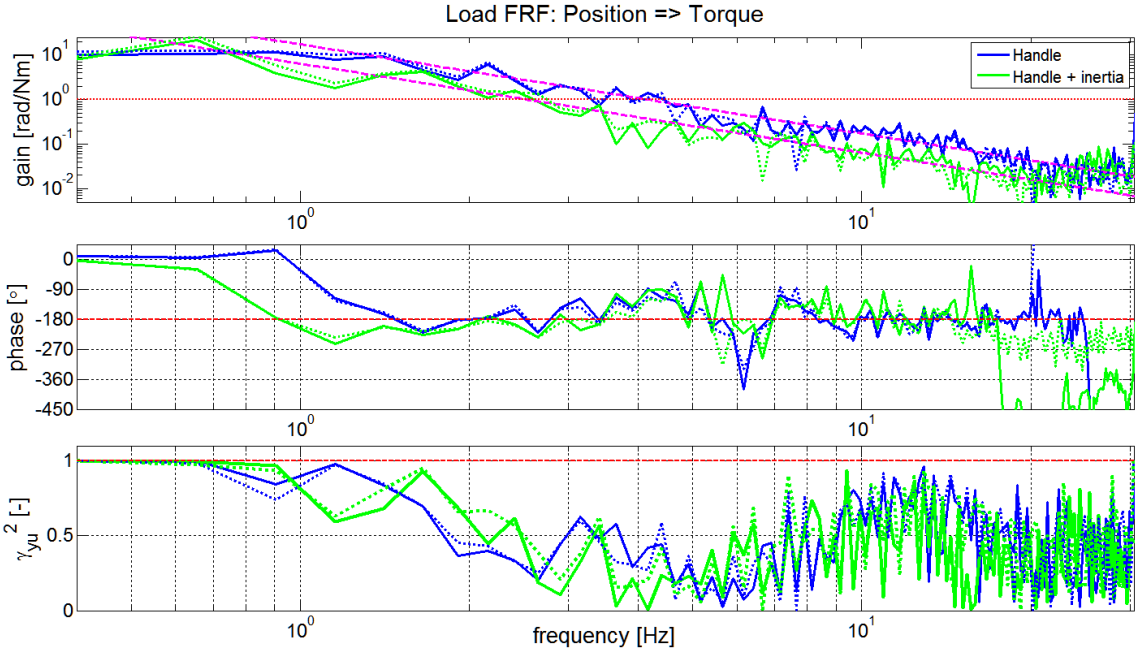

Figure 4.7: The load FRFs of the position input to the torque output. For comparison, the FRFs are also determined with the measurements from the conventional position sensor (dashed lines), the solid lines are made with use of the optical position sensor. The FRFs are averaged over 4 repetitions and to improve the estimates, the spectral densities were averaged over 4 frequency bands. The dashed magenta lines are the theoretical FRFs for the load inertia's.

5 Discussion

In this paper, a design for an MR-safe haptic wrist manipulator suited for proprioceptive reflex identification is presented. After the design a proof-of-concept prototype was made which resulted in a custom-made MR-safe prototype with electro-hydraulic actuation, an optical position sensor and an optical torque sensor. All used materials inside the MR-environment are electrical non-conductive and magnetically compatible. Of the vane motor two iterations were made. The first suffered from stick-slip friction and had a single vane. The second iteration had reduced friction and a double vane so that the axis of the rotor was loaded with a couple instead of a moment. This results in less deformation of the rotor axis and thus less friction between stator and rotor. Furthermore a couple provides twice the torque, given the same actuator dimensions. The vane motor's range of motion is from -67° to 67° (134° total) and has a designed torque delivery of 8 Nm at a 3 bar pressure difference. Furthermore, no distortions in the MR-image or distortions in the sensor signal from the manipulator were observed during a test in an MR-scanner (AMC, Amsterdam).

5.1 MR-safe

Whether a material is MR-safe is debatable because of how it is determined. An item is deemed MR-safe by providing a scientifically based rationale rather than test data. This means that conducting magnetic compatible materials, such as aluminum, which are not susceptible for induced force or torques but are susceptible for induced eddy currents are cause for debate. Induced eddy currents can cause heating of the material (safety hazard) and a local magnetic field which deteriorates fMRI image quality. Thus suggesting that conducting magnetically compatible materials are not MR-safe. However, when conducting magnetically compatible materials are used outside the bore, on non-moving parts and it is impossible for the subjects to become part of a conductive loop, then there is no direct safety hazard and image quality is not necessarily compromised. Nevertheless, to avoid discussion, in this design the choice is made to only use electrical non-conductive and magnetically compatible materials, such as plastics, glass and rubber. As a result the fMRI quality is ensured and the manipulator is suited for safe use in any MR-environment.

5.2 Design

Material, production technique & sealing
The first iteration of the vane motor had an O-ring seal which provided a good seal and allowed pre-pressure, but suffered severely from stick-slip friction. After consulting an expert from a seal manufacturer (Eriks, Alkmaar, The Netherlands) the second iteration of the vane motor had an X-ring seal which would reduce the amount of stick-slip. The second iteration of the vane motor did not suffer from stick-slip but there was some leakage along the axis of the vane motor. Possibly caused by the limited accuracy of rapid prototype techniques. The accuracy of the used rapid prototype techniques was $\pm 0.2\%$ (min ± 0.2 mm) which resulted in large tolerances. A different fabrication technique could provide a higher accuracy, however the internal ducts of the vane motor exclude many other production techniques. A possible solution would be to use rapid prototype techniques

with larger part dimension so that finishing can be performed with conventional milling machine and lathe to improve the accuracy. Different X-ring and O-ring seals were used that according to the dimension of the axis and cover hole should provide seal. Possibly the surface finish of the materials or the shape accuracy of the holes are cause for the leakage. After fitting the largest available O-ring, there was no noticeable stick-slip friction and the leakage was reduced to an acceptable amount for testing. However the leakage did prevent the use of pre-pressure in the system which reduced the maximum torque and bandwidth performance of the prototype.

Maximum torque
The vane motor was unable to deliver its designed torque at a pressure difference of 3 bar because of cavitation at inlet of the pump. Since with the current prototype pre-pressure was not a possibility, the pressure at the inlet pump became too low and caused cavitation resulting in a free turning pump. This limited the achieved torque to 1.5 Nm, which still was enough to met the requirement of 1.2 Nm. This limitations will be resolved in a next iteration of the vane motor with adjusted axis sealing and use of pre-pressure.

Bearings
In the design of the vane motor plastic ball bearings with a PEEK cage and glass balls from Igus (Xirodur A500) were used. These bearings had more radial play than expected, compressing the bearing in radial direction reduces the axial play. However the used fabrication technique did not allow for a tight fit which would reduce the amount of radial play. Reduced radial play permits a smaller gap between the rotor and the stator, reducing the amount of internal leak without the risk of increased friction under load.

Sensors
The sensors in the prototype have fibers which were 5 meters long, since that was the maximum length available from the manufacturer. However a minimal length of 9 meters is required to reach the control room in an MR-environment. A specialized custom fabrication of the used sensor heads with fibers of 9 meters long should be possible and is expected not to prove any significant increased signal loss compared to the 5 meter long fibers. The torque sensor has an achieved accuracy of $\pm 2\%$ full scale (F.S. = 14.3 Nm). Further testing when the control of the system is improved will tell if this is sufficient. However, the focal point distance of the sensor and the edge of the detection area are of great influence on the performance of the sensor. The performance of the torque sensor will increase with the improved accuracy of the manufacturing of the deformable body. The achieved accuracy for the position sensor was sufficient, being $\pm 1\%$ full scale (F.S. = 70°=1.22 rad) in relation to the conventional sensor. The workspace of the prototype was limited to -35° to 35° due to the dimension of the encoder disc. At the ends of the planned range of motion, the reflective surface was either too little or too great resulting in an inaccurate signal. In a new encoder disk the usable surface needs to be redistributed over a larger range of motion. For the assessment of the manipulator the currently achieved workspace of $\pm 35^\circ$ was sufficient. The used design for the encoder disc is a circle with an eccentric hole. This results in a non-linear distribution of the reflective surface over the range of motion. Instead of a circle, a specific curved shape provides a linear distribution of the reflective surface over the range of motion. However since this fabrication of such a curved shape requires the use of a x-y table, it will result in an edge with discrete steps. For the prototype the circle was chosen as encoder disc because it can be constructed on a lathe which results in a continuous edge and the non-linear distribution of reflective surface can be easily accounted for in the control of the system.

Control
Controlling the system accurately over the desired bandwidth (20 Hz) with a PI controller was not successful due to the inherent non-linearities of hydraulics. Attempts to improve control performance by adding a parallel feed forward gain to the commanded velocity to compensate for the internal leak of the vane motor and a compensation gain for the static coulomb friction did not result in satisfactory results. However during tuning of the PI controller good position tracking results for 1 and 2 Hz sine motions were obtained, which showed no signs of stick-slip friction. Furthermore even with the axis leakage and lack of pre-pressure an open-loop bandwidth (-3 dB or $\sqrt{0.5} \approx 0.707$ gain) of approximately 5 Hz and -180 $^\circ$ phase passing at 7 Hz was achieved. The results of the impedance FRFs showed that it was already possible to estimate the tested inertial loads in the same order of magnitude. With the implementing of model-based control in future work, the control performance of the system will be improved and a higher bandwidth achieved.

5.3 Recommendations

Pre-pressure
One of the next steps for the MR-compatible haptic manipulator should be to make sure that pre-pressure of the system is possible. This will improve the bandwidth and maximum producible torque. To make pre-pressure possible the leakage around the axis must be remedied by looking at different or additional fabrication techniques to improve the accuracy of the parts. Furthermore a lip-seal is the preferred sealing for low-pressure dynamic rotary movement. This type of seal was not used because it has a metal housing, however a custom-made lip-seal can be constructed out of plastic. The fabrication time of such a custom plastic lip-seal was 10 weeks minimal and could therefore not be implemented in the prototype. Leakage across an O-ring is often caused by entrained air (aeration) in the fluid, i.e. small air bubbles typically with a diameter of less than 1 mm dispersed throughout the fluid. One percent of entrained air can reduced a fluid's bulk modulus by 25 percent. Since the stiffness of a fluid is related to it's bulk modulus, less entrained air will be beneficial for the bandwidth. It is recommended to look for possible alternative fluids with better aeration properties, however the fluid must still remain non-toxic and non-corrosive. Increasing the reservoir size and placing the inlet and outlet ports further apart also reduces the change of small air bubbles being fed back into the system.

Position sensor
The range of motion of the position sensor can be improved by creating a new encoder disk which divides the usable reflected surface over a larger range.

Control
The control of the system will be improved by implementing an inverse model of the system (Otten et al., 2011). It is thus recommended to create an accurate model of the system and implement a model-based controller.

MR-facilities
Since the combination of an MR-safe manipulator and MR-scanner is a valuable tool with numerous opportunities in view, the demand for MR-compatible devices will grow. To ensure MRI quality and MR-safety many current MR-compatible devices use a transmission to transfer mechanical energy from the control room to the MR-environment.

Currently that distance is 9 m for most MR-facilities. However if that distance were to be reduced, so would many disadvantages and limitations of long transmission. It is therefore recommended to take this into account while building new MR-facilities by reducing the distance between control room and MR-environment. Placing an access panel close to the MR-scanner will expand the possibilities and development of MR-compatible devices. However, until that time, with the implementation of the other recommendations, the presented design of an MR-safe haptic manipulator is expected to be suited for proprioceptive reflex identification in current MR-facilities.

5.4 Applications

Proprioceptive reflex identification is motion control research with one of the most stringent demands regarding the haptic manipulator. Besides proper tremor diagnosis, combining an MR-scanner and the MR-safe haptic manipulator, will allow for other types of motor control research during which fMRI will enable to see which parts of the brain are active. E.g. sensory weighting, repeatable force-controlled motor tasks, goal-directed motor task. Investigating how the brain changes over time while learning a motor task improves the understanding of brain circuits involved in normal motor learning and in cortical remapping: the brain's ability to replace damaged neural pathways following a neurological injury (Tsekos et al., 2007; Rowe and Frackowiak, 1999). The combination of fMRI and proprioceptive reflex identification will potentially provide insights into brain function, functional and dysfunctional motor control and the regeneration process after a nerve lesion, making this combination of techniques a valuable tool for neuroscientists and technicians (Gassert et al., 2008b; Heeger and Ress, 2002; Yu et al., 2008).

5.5 Conclusion

The main challenge was designing a manipulator that would function safely in any MR-environment during fMRI without compromising the image quality. This challenge is accomplished by using electro-hydraulic actuation and MR-safe optical sensors and vane motor (end effector). During a test in an MR-scanner no distortions in the MR-image and no distortions in the sensor signal were observed. With an achieved range of motion of $\pm 67^\circ$ and produced torque of 1.5 Nm the requirements of $\pm 40^\circ$ and 1.2 Nm are fulfilled and a smooth motion without stick-slip is realized. The performance of the prototype was reduced by leakage across the vane motor axis and limited control performance of the PI controller. However typical responses were obtained with impedance FRFs of two inertial loads. Furthermore, even with leakage and without pre-pressure, the open-loop FRF of the commanded velocity to the measured vane velocity had a measured bandwidth (-3 dB or $\sqrt{0.5} \approx 0.707$ gain) of approximately 5 Hz and a -180 $^\circ$ phase passing at 7 Hz. Although the bandwidth does not fulfill the requirement for proprioceptive reflex identification it does allow for various motor control experiments. With the recommendations carried out, it is expected that the next prototype will also be suited for proprioceptive reflex identification during fMRI.

Acknowledgements

The Movement Diagnostic System
The designed MR-safe haptic manipulator is part of a larger project which also entails an electromyography (EMG) system to record muscle activations and a motion tracking system to record the movement during fMRI using cameras and accelerometers for additional information which can aid in identifying anomalies and image artifacts. Analyzing the peripheral and central components of tremor in patients by realizing and applying a system that combines fMRI images of the brain, measurements of muscle activation (EMG), a video tracking device and a haptic manipulator to manipulate the neural motor control system is the goal of Neurosipe project 10739: The Movement Diagnostic System (MDS)[1].

[1] `http://neurosipe.nl/project.php?id=25`

Appendices

A Design

Actuator

The maximum width, or outer diameter in Figure A.1, the vane motor actuator is permitted to have is chosen at 120 mm (Section 2.1). To reduce the chance of leakage and with safety regards take into account, the maximum pressure difference was set at 3 bar. For the side walls of the stator a minimal width of 10 mm is needed for the required space for the O-ring seal and screw holes for the cover.

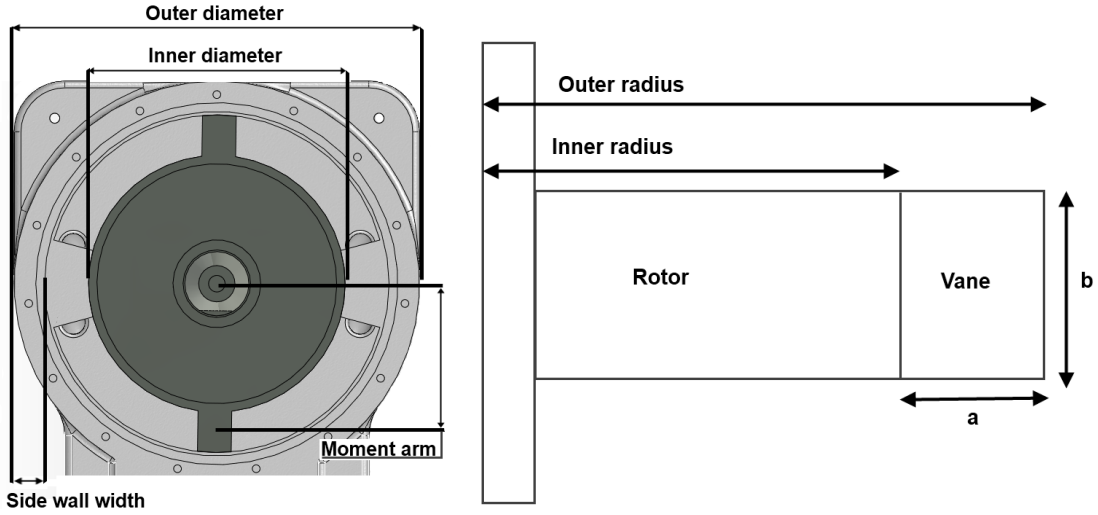

(a) Top view of the vane motor, indicated are the dimensions of interest.

(b) Cross-sectional drawing of half the rotor.

Figure A.1: Overview of the dimensions of interest in the design of the vane motor.

For a certain torque requirement (M), an increased moment arm (r) will reduce the required force. The needed amount of vane area will thus also be reduced, given a maximum fixed pressure difference of 3 bar. Since the leak across the vane is assumed to be related to the vane perimeter, a reduced vane area will reduce the perimeter and thus the leakage. In Figure A.1b the perimeter has a length of, $L = 2 \cdot a + b$. In Equation A.1 the vane area (A) is assumed square, so $b = a$.

$$
\begin{aligned}
&M = F \cdot r && \text{F= force, P = pressure, r = moment arm} \\
&M = (P \cdot A) \cdot r \\
&{}^{M}/_{P} = A \cdot r = 2 \cdot a^2 \cdot r \\
&a^2 = \tfrac{M}{P} \cdot \tfrac{1}{2 \cdot r} && {}^{M}/_{P} = \text{assumed constant and leak} \equiv a \\
&\text{leak} \equiv a \equiv \sqrt{\tfrac{M}{P} \cdot \tfrac{1}{2 \cdot r}} \\
&\text{leak} \equiv \tfrac{1}{\sqrt{2 \cdot r}}
\end{aligned}
\tag{A.1}
$$

So with increased moment arm the leak decreases for a given amount of required torque (M). The optimal ratio between the area and perimeter would result in a half round vane. However, then it would not be possible to assemble the rotor into the stator. By iteration the needed area for a vane was determined to be approximately 300 mm^2.

$$
\begin{aligned}
&L = 2 \cdot a + b && , A = a \cdot b \qquad \text{A= constant = 300 mm}^2 \\
&L = 2 \cdot \tfrac{A}{b} + b \\
&L' = -2A \cdot \tfrac{1}{b^2} + 1 \\
&L' = 0 \rightarrow 1 = 2A \cdot \tfrac{1}{b^2} \\
&b^2 = 2A = 2 \cdot (a \cdot b) \quad \rightarrow 2a = b
\end{aligned}
\tag{A.2}
$$

The ratio between a and b should be 1 : 2. The dimensions of the vane were thus chosen to be a = 12.5 mm and b = 25 mm. The resulting area and remaining moment arm are then respectively 312.5 mm^2 and 43.75 mm. At a pressure of 3 bar (0.3 $^{\text{N}}/_{\text{mm}^2}$ this gives a torque of $2 \cdot 312.5 \cdot 0.3 \cdot {}^{43.75}/_{1000} = 8.2$ Nm.

Tubing and fluid
The used hydraulic transmission can be modelled as a spring with stiffness (Ganesh et al., 2004):

$$K \equiv \frac{B \cdot A}{L}$$

Where $B[Pa]$ is the Bulk modulus of the fluid, $A[m^2]$ the cross-sectional area and $L[m]$ the length of the tube. The stiffness increases with A and B and decreases with L. However as concluded by Ganesh et al. (2004) the influence of the cross-sectional area on the bandwidth is negligible as the fluid inertia also increases with the diameter. The natural frequency was found to be independent of the tube diameter. More important is the amount of entrained air (aeration) in the fluid, i.e. small air bubbles typically with a diameter of less than 1 mm dispersed throughout the fluid, one percent of entrained air can reduce the Bulk modulus by 25%.

Sensors

For both the position sensor and the torque sensor the Keyence FS-N11MN amplifier is used. This amplifier has an output from 1 to 5 volt with a repeat precision of $\pm 0.5\%$. The amplifiers were used in the *Turbo* mode resulting in a 12 bit output range and response time of 1 ms.

Torque sensor
The optical sensor head for the torque sensor is a Keyence FU-38. The focal length for this sensor head is 6 mm with a spot diameter of 1.5 mm. Testing showed that the measurable translation of this sensor head with the knife-edge method was 0.30 mm. With the use of SolidWorks simulation the deformable body is dimensioned such that the translation of the reflective surface is ± 0.15 mm with a applied torque of ± 8 Nm, resulting in a measurement range of 16 Nm.

Position sensor
For the position sensor the Keyence FU-37 optical sensor head was used, which has detection area of 4.5 mm by 3.5 mm with a focal length of 3 mm. The encoder disc was dimensioned such that the reflective area changed in the direction of the 4.5 mm of the sensor head's detention area. The reflective area was linear dived to match the vane motor's range of motion, resulting in 0.5 mm overlap for minimal reflection to 4.5 mm overlap for maximal reflection.

Inertia calculations

The inertia of the loads used to measure the impedance FRFs are calculated with SolidWorks. A manual calculation for the handle inertia gives similar results. In the manual calculation the sensor body is assumed a rod of length L with the axis of rotation at the end and the handle a point mass at distance L. The masses are obtained via SolidWorks.

$$I_A = m \cdot L^2$$

$$I_A = 117g \cdot (\frac{91mm}{1000})^2 = 0.968gm^2$$

$$I_B = \frac{m \cdot L^2}{3}$$

$$I_B = \frac{170g \cdot (\frac{91mm}{1000})^2}{3} = 0.469gm^2$$

$$I_{handle} = I_A + I_B = 1.44gm^2$$

$$I_{yy} = 1.46 \text{ g m}^2$$

Mass properties of Assem1 (Assembly Configuration - Default)

Output coordinate System: -- default --

The center of mass and the moments of inertia are output in the coordinate system of Assem1
Mass = 284.14 grams

Volume = 194598.72 cubic millimeters

Surface area = 52694.23 square millimeters

Center of mass: (millimeters)
X = -56.00
Y = 35.85
Z = 0.04

Principal axes of inertia and principal moments of inertia: (grams * square millimeters)
Taken at the center of mass.
Ix = (0.76, -0.65, 0.00) Px = 270747.44
Iy = (0.65, 0.76, 0.00) Py = 788539.02
Iz = (-0.00, -0.00, 1.00) Pz = 917939.75

Moments of inertia: (grams * square millimeters)
Taken at the center of mass and aligned with the output coordinate system.
Lxx = 488880.77 Lxy = -255666.49 Lxz = 876.20
Lyx = -255666.49 Lyy = 570407.83 Lyz = -263.04
Lzx = 876.20 Lzy = -263.04 Lzz = 917937.62

Moments of inertia: (grams * square millimeters)
Taken at the output coordinate system.
Ixx = 853969.92 Ixy = -825999.37 Ixz = 306.28
Iyx = -825999.37 Iyy = 1461368.45 Iyz = 101.79
Izx = 306.28 Izy = 101.79 Izz = 2173986.66

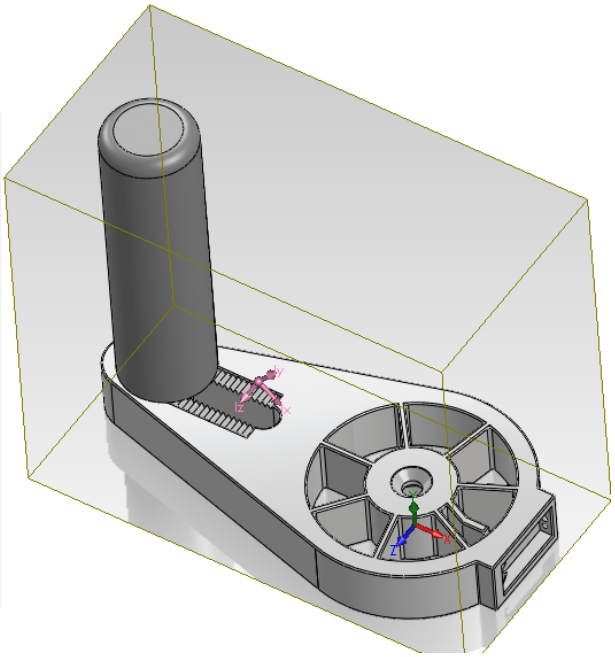

Figure A.2: SolidWorks calculation of the handle inertia.

$$I_{yy} = 3.93\ \mathrm{g\,m^2}$$

Mass properties of Assem1 (Assembly Configuration - Default)

Output coordinate System: -- default --

Mass = 764.14 grams

Volume = 256927.92 cubic millimeters

Surface area = 65863.79 square millimeters

Center of mass: (millimeters)
X = -64.04
Y = 51.02
Z = 0.01

Principal axes of inertia and principal moments of inertia: (grams * square millimeters)
Taken at the center of mass.
Ix = (-0.60, 0.80, -0.00) Px = 563896.13
Iy = (-0.80, -0.60, -0.01) Py = 1210927.94
Iz = (-0.01, -0.01, 1.00) Pz = 1249488.78

Moments of inertia: (grams * square millimeters)
Taken at the center of mass and aligned with the output coordinate system.
Lxx = 977016.47 Lxy = -310863.54 Lxz = 958.06
Lyx = -310863.54 Lyy = 797815.68 Lyz = -417.47
Lzx = 958.06 Lzy = -417.47 Lzz = 1249480.70

Moments of inertia: (grams * square millimeters)
Taken at the output coordinate system.
Ixx = 2965969.91 Ixy = -2807439.36 Ixz = 306.28
Iyx = -2807439.36 Iyy = 3931570.04 Iyz = 101.79
Izx = 306.28 Izy = 101.79 Izz = 6372188.24

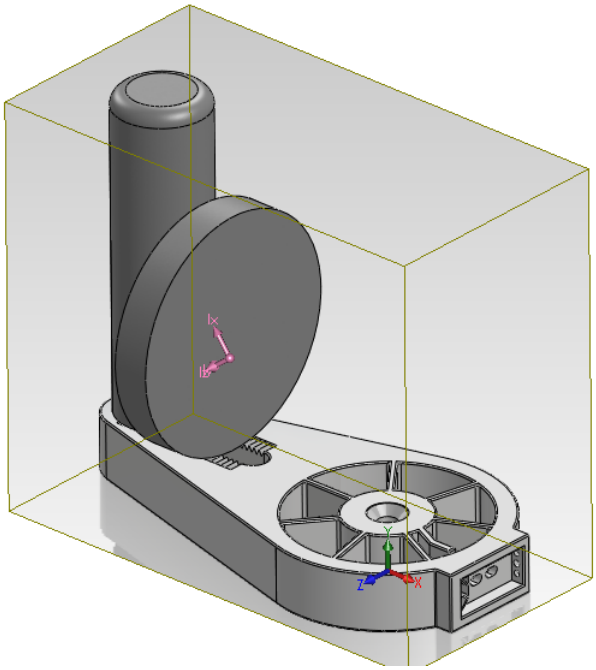

Figure A.3: SolidWorks calculation of the handle and weight inertia.

B Photos

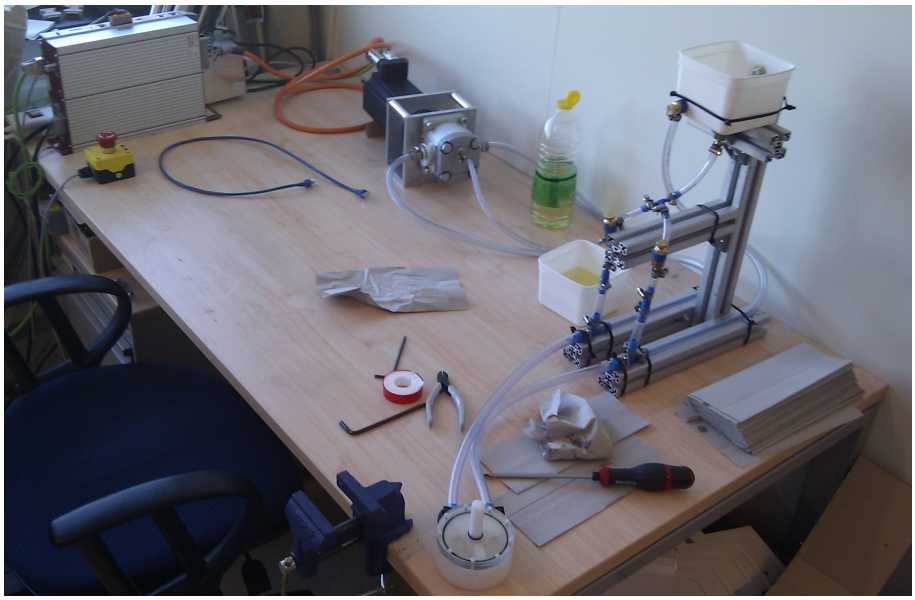

Figure B.1: Overview photo of first test setup with first vane motor prototype and 1.5 m tubes.

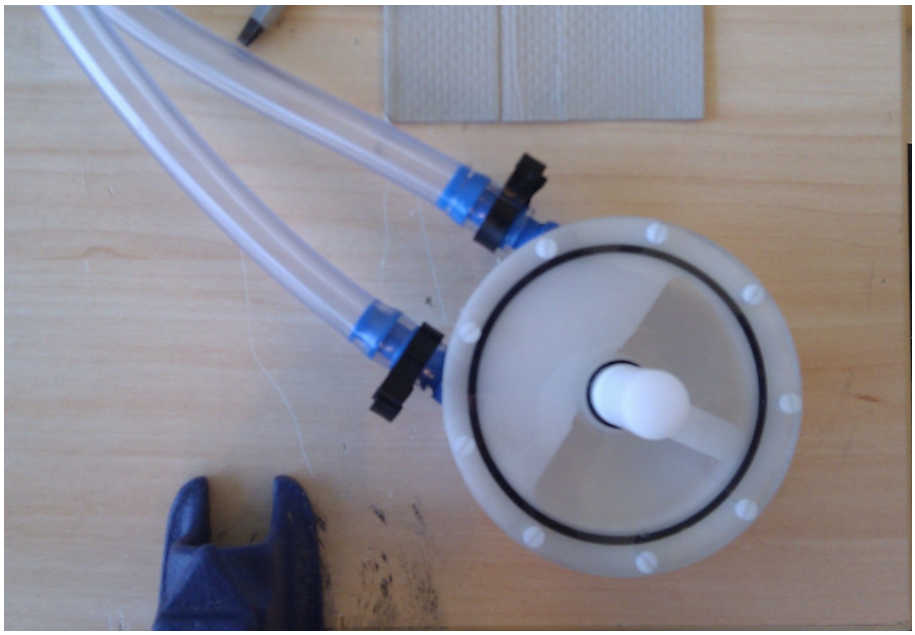

Figure B.2: Photo of the first vane motor prototype.

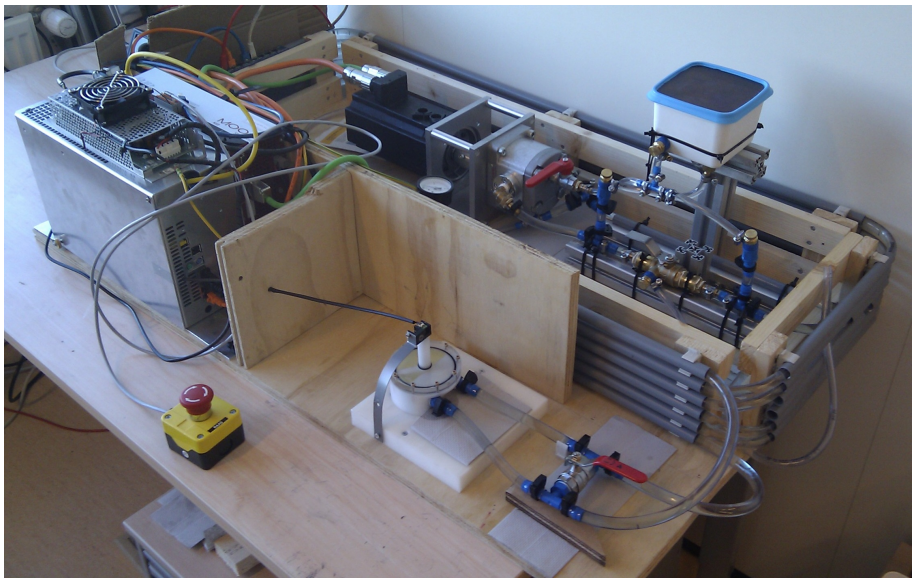

Figure B.3: Overview photo of second test setup with first vane motor prototype and tubes increased to 2 x 9 m.

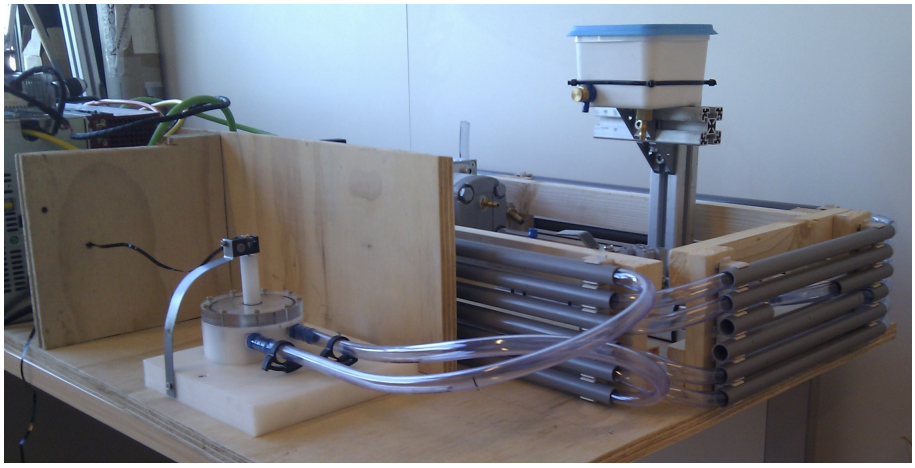

Figure B.4: Close up of the first prototype vane motor with conventional position sensor placed for testing purposes.

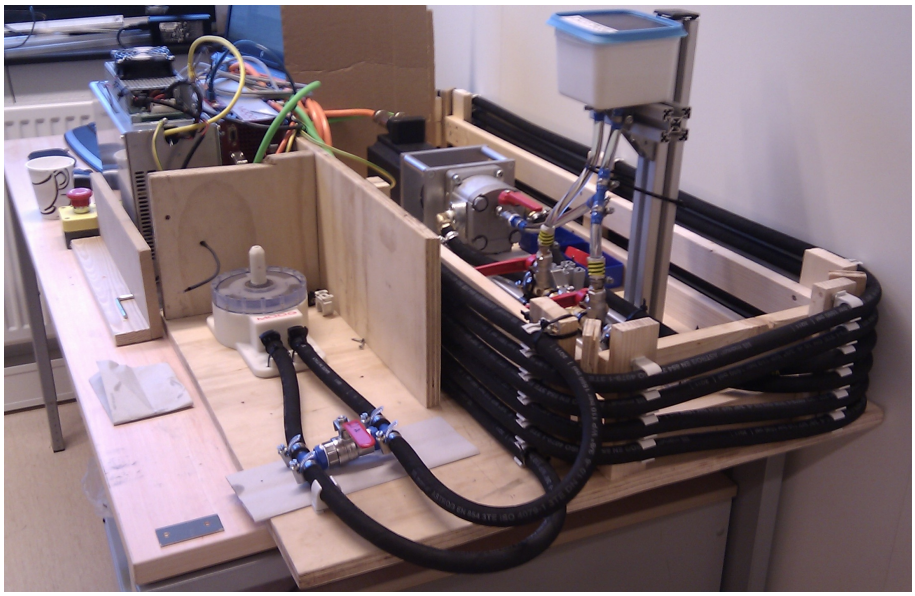

Figure B.5: Overview photo of third an final test setup with second vane motor prototype and new less compliant tubes (2 x 9 m).

Figure B.6: Photo of the second and last prototype of the vane motor before assembly.

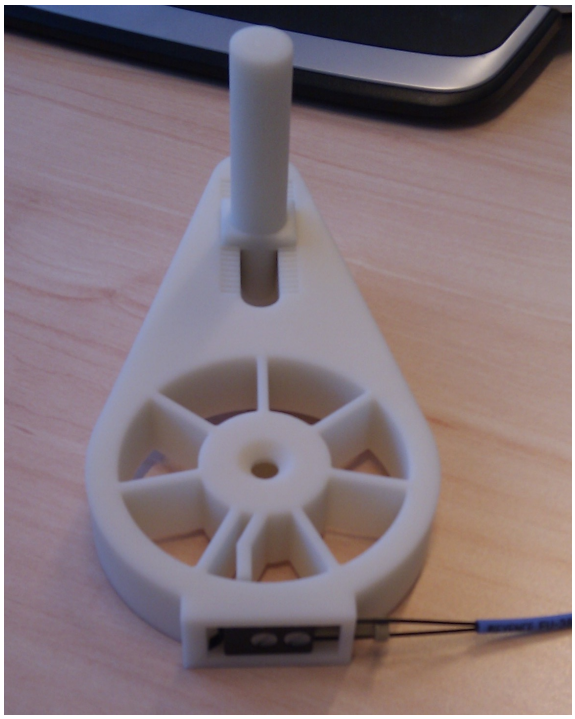

Figure B.7: Photo of the torque sensor with the optical Keyence sensor head placed.

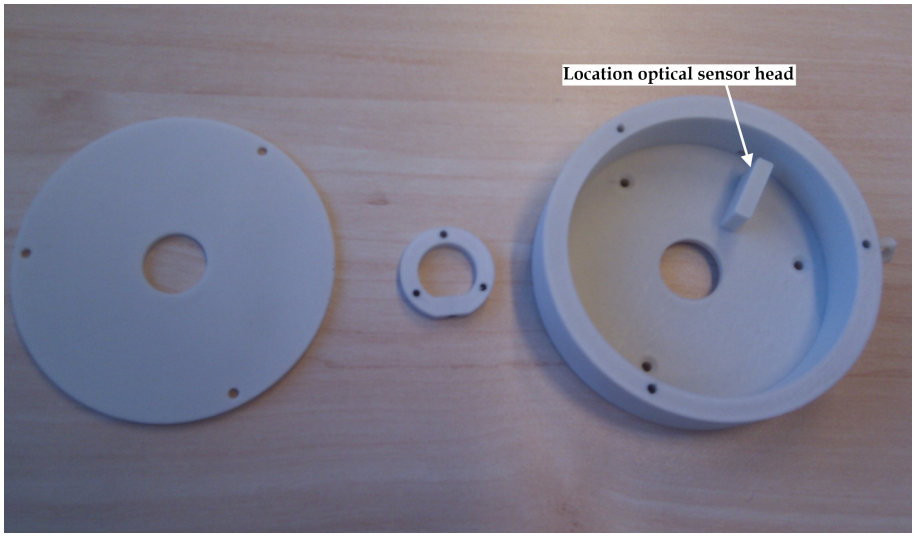

Figure B.8: Photo of the position sensor housing. From left to right are seen: the cover, the ring to attach the encoder disc an the base housing.

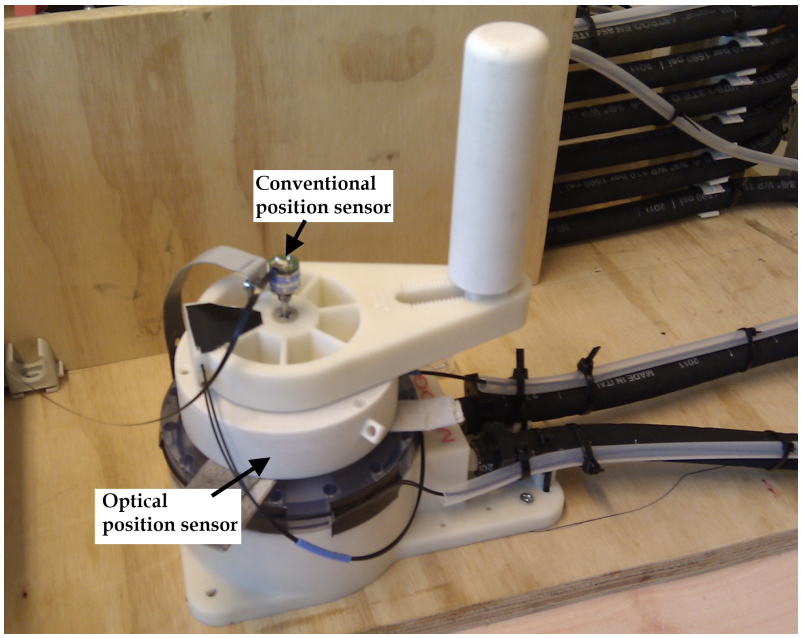

Figure B.9: Photo of the calibration setup for the optical position sensor with use of a conventional sensor, both sensor are indicated.

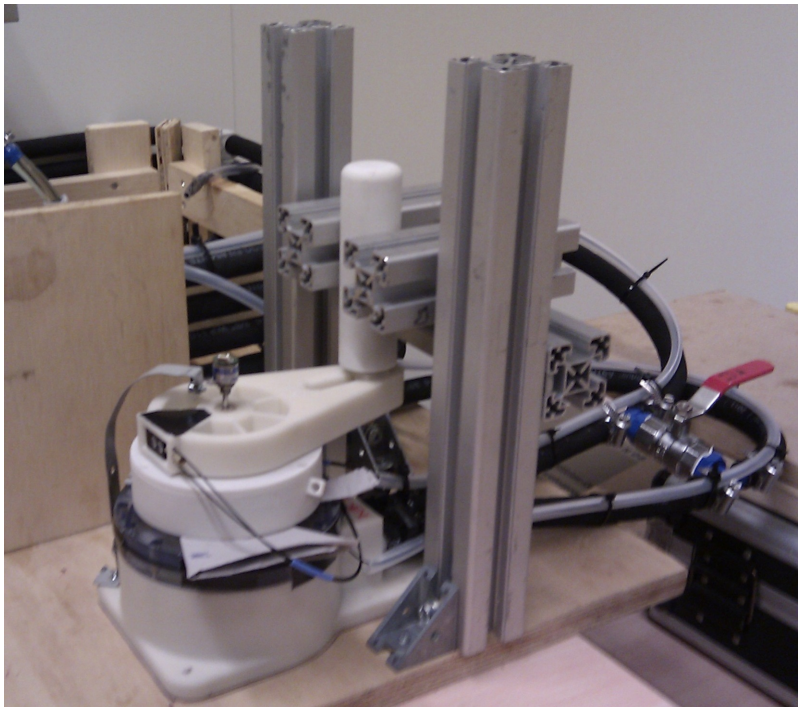

Figure B.10: Photo of the test setup used to fixated the handle for the maximum producible torque tests.

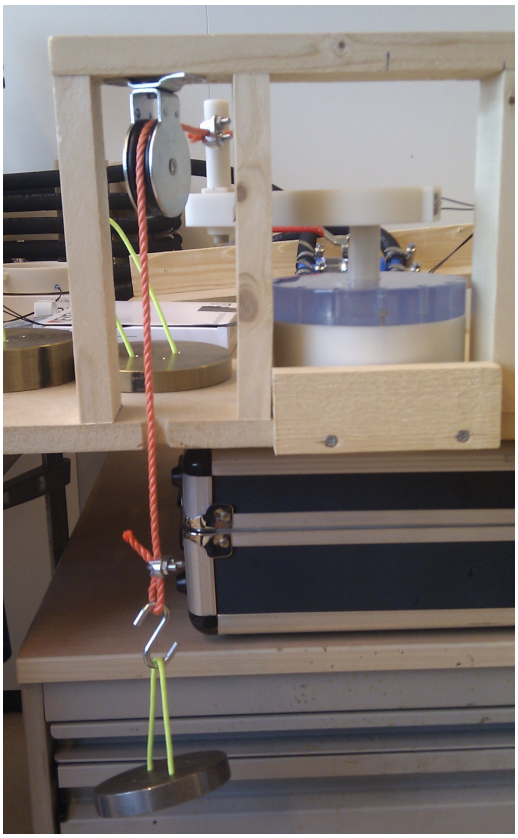

Figure B.11: Photo of the calibration setup for the optical torque sensor.

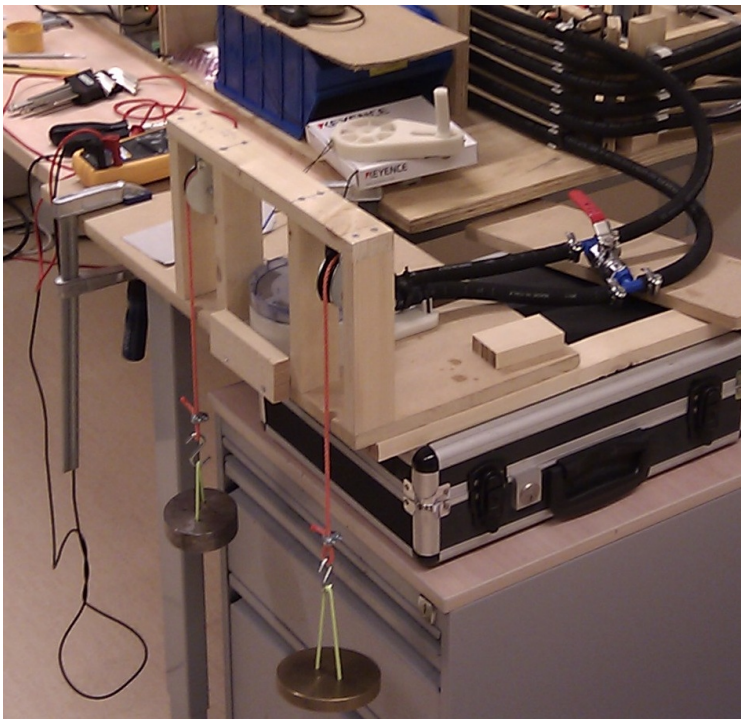

Figure B.12: Photo of the calibration setup for the optical torque sensor.

Figure B.13: Photo of the test in an MR-scanner (AMC, Amsterdam). No distortions in the MR-image or distortions in the sensor signal were observed.

References

ASTM. Standard practice for marking medical devices and other items for safety in the magnetic resonance environment. *F2503-08*, 2008. 2.1

Etienne Burdet, Roger Gassert, Ganesh Gowrishankar, Dominique Chapuis, and Hannes Bleuler. fmri compatible haptic interfaces to investigate human motor control. *Experimental Robotics IX*, 21:25–34, 2006. 2.2

Wiliam D. Calister. *Materials Sience and Engineering An Introduction*. John Wiley & Sons, Inc., 2003. 3.3

D. Chapuis, R. Gassert, L. Sache, E. Burdet, and H. Bleuler. Design of a simple mri/fmri compatible force/torque sensor. In *Intelligent Robots and Systems, 2004. (IROS 2004). Proceedings. 2004 IEEE/RSJ International Conference on*, volume 3, pages 2593 – 2599 vol.3, 2004. doi: 10.1109/IROS.2004.1389799. 2.3

D. Chapuis, R. Gassert, G. Ganesh, E. Burdet, and H. Bleuler. Investigation of a cable transmission for the actuation of mr compatible haptic interfaces. In *Biomedical Robotics and Biomechatronics, 2006. BioRob 2006. The First IEEE/RAS-EMBS International Conference on*, pages 426 –431, feb. 2006. doi: 10.1109/BIOROB.2006.1639125. 2.2

K. Chinzei, R. Kikinis, and F.A. Jolesz. Mr compatibility of mechatronic devices: Design criteria. 2:1020–1031, 09 1999. 2.2

Eftychios G. Christoforou, Nikolaos V. Tsekos, and Alpay Özcan. Design and testing of a robotic system for mr image-guided interventions. *J. Intell. Robotics Syst.*, 47:175–196, October 2006. ISSN 0921-0296. doi: 10.1007/s10846-006-9082-0. URL `http://dl.acm.org/citation.cfm?id=1166879.1176995`. 2.1, 2.2, 3.1

E. de Vlugt, A.C. Schouten, F.C.T. van der Helm, P.C. Teerhuis, and G.G. Brouwn. A force-controlled planar haptic device for movement control analysis of the human arm. *J Neurosci Methods*, 129(2):151–68, 2003. 2.1

Erwin de Vlugt, Alfred C. Schouten, and Frans C. T. van der Helm. Adaptation of reflexive feedback during arm posture to different environments. *Biological Cybernetics*, 87: 10–26, 2002. ISSN 0340-1200. URL `http://dx.doi.org/10.1007/s00422-002-0311-8`. 10.1007/s00422-002-0311-8. 1.1

G. Deuschl, P Bain, and M. Brin. Consensus statement of the movement disorder society on tremor. *Movement Disorders*, 13:2–23, 1998. 1.1

G. Deuschl, R. Wenzelburger, K. Laffler, J. Raethjen, and H. Stolze. Essential tremor and cerebellar dysfunction clinical and kinematic analysis of intention tremor. *Brain*, 123(8):1568–1580, 2000. doi: 10.1093/brain/123.8.1568. URL `http://brain.oxfordjournals.org/content/123/8/1568.abstract`. 1.1

R.J. Elble. Central mechanisms of tremor. *Jour. of Clinical Neurophysiology*, 13:133–144, 1996. 1.1

RJ. Elble and G. Deuschl. *Tremor*. Philadelphia: WB Saunders CO., 2002. 1.1

H. Elhawary, A. Zivanovic, M. Rea, B.L. Davies, C. Besant, I. Young, and M.U. Lamperth. A modular approach to mri-compatible robotics. *Engineering in Medicine and Biology Magazine, IEEE*, 27(3):35 –41, may-june 2008. ISSN 0739-5175. doi: 10.1109/EMB.2007.910260. 2.2

M. Flueckiger, M. Bullo, D. Chapuis, R. Gassert, and Y. Perriard. fmri compatible haptic interface actuated with traveling wave ultrasonic motor. In *Industry Applications Conference, 2005. Fourtieth IAS Annual Meeting. Conference Record of the 2005*, volume 3, pages 2075 – 2082 Vol. 3, oct. 2005. doi: 10.1109/IAS.2005.1518734. 2.2, 2.3

G. Ganesh, R. Gassert, E. Burdet, and H. Bleuler. Dynamics and control of an mri compatible master-slave system with hydrostatic transmission. In *Robotics and Automation, 2004. Proceedings. ICRA '04. 2004 IEEE International Conference on*, volume 2, pages 1288 – 1294 Vol.2, 26-may 1, 2004. doi: 10.1109/ROBOT.2004.1308002. A

R. Gassert, R. Moser, E. Burdet, and H. Bleuler. Mri/fmri-compatible robotic system with force feedback for interaction with human motion. *Mechatronics, IEEE/ASME Transactions on*, 11(2):216 –224, april 2006. ISSN 1083-4435. doi: 10.1109/TMECH.2006.871897. 2.1, 2.2, 2.2, 2.3

R. Gassert, E. Burdet, and K. Chinzei. Mri-compatible robotics. *Engineering in Medicine and Biology Magazine, IEEE*, 27(3):12 –14, may-june 2008a. ISSN 0739-5175. doi: 10.1109/EMB.2007.910273. 2.1

R. Gassert, E. Burdet, and K. Chinzei. Opportunities and challenges in mr-compatible robotics. *Engineering in Medicine and Biology Magazine, IEEE*, 27(3):15 –22, may-june 2008b. ISSN 0739-5175. doi: 10.1109/EMB.2007.910265. 5.4

G. Grimaldi and M. Manto. *'Tremor: From pathogenesis to Treatment'*. Morgan & Claypool, 2008. 1.1

Giuliana Grimaldi, Piet Lammertse, Niels Van Den Braber, Jos Meuleman, and Mario Manto. A new myohaptic device to assess wrist function in the lab and in the clinic the wristalyzer. *EuroHaptics LNCS*, pages 33–42, 2008. 2.1

DJ. Heeger and D. Ress. What does fmri tell us about neuronal activity? *Nature Reviews Neuroscience*, 3:142–151, 2002. 5.4

J. Hidler, J. Mbwana, and T. Zeffiro. Mri compatible force sensing system for real-time monitoring of wrist moments during fmri testing. In *Rehabilitation Robotics, 2005. ICORR 2005. 9th International Conference on*, pages 212 – 214, june-1 july 2005. doi: 10.1109/ICORR.2005.1501087. 2.3

J Jankovic. Parkinsons disease: clinical features and diagnosis. *Journal of Neurology, Neurosurgery & Psychiatry*, 79(4):368–376, 2008. doi: 10.1136/jnnp.2007.131045. URL `http://jnnp.bmj.com/content/79/4/368.abstract`. 1.1

Emanuel Kanal, A. James Barkovich, Charlotte Bell, James P. Borgstede, William G. Bradley, Jerry W. Froelich, Tobias Gilk, J. Rod Gimbel, John Gosbee, Ellisa Kuhni-Kaminski, James W. Lester, John Nyenhuis, Yoav Parag, Daniel J. Schaefer, Elizabeth A. Sebek-Scoumis, Jeffrey Weinreb, Loren A. Zaremba, Pamela Wilcox, Leonard Lucey, Nancy Sass, and the ACR Blue Ribbon Panel on MR Safety. Acr guidance document for safe mr practices: 2007. *American Journal of Roentgenology*, 188(6):1447–1474, 2007. doi:

10.2214/AJR.06.1616. URL http://www.ajronline.org/content/188/6/1447.short. 2.1

Eric R. Kandel, James H. Schwartz, and Thomas M. Jessell. *Principles of neural science*. New York : McGraw-Hill, Health Professions Division, 4th edition edition, 2000. 1.1

R.E. Kearney, R.B. Stein, and L. Parameswaran. Identification of intrinsic and reflex contributions to human ankle stiffness dynamics. *Biomedical Engineering, IEEE Transactions on*, 44(6):493 –504, june 1997. ISSN 0018-9294. doi: 10.1109/10.581944. 1.1

Azadeh Khanicheh, Andrew Muto, Christina Triantafyllou, Brian Weinberg, Loukas Astrakas, Aria Tzika, and Constantinos Mavroidis. fmri-compatible rehabilitation hand device. *Journal of NeuroEngineering and Rehabilitation*, 3:1–11, 2006. ISSN 1743-0003. URL http://dx.doi.org/10.1186/1743-0003-3-24. 10.1186/1743-0003-3-24. 2.2, 2.3

J.Z Liu, T.H Dai, T.H Elster, V Sahgal, R.W Brown, and G.H Yue. Simultaneous measurement of human joint force, surface electromyograms, and functional mri-measured brain activation. *Journal of Neuroscience Methods*, 101(1):49 – 57, 2000. ISSN 0165-0270. doi: 10.1016/S0165-0270(00)00252-1. URL http://www.sciencedirect.com/science/article/pii/S0165027000002521. 2.3

ED Louis and JP Vonsattel. The emerging neuropathology of essential tremor. *Movement Disorders*, 23:174 – 182, 2008. 1.1

Hara Masayuki, Matthey Gaetan, Yamamoto Akio, Chapuis Dominique, Gassert Roger, Bleuler Hannes, and Higuchi Toshiro. Development of a 2- dof electrostatic haptic joystick for mri/fmri applications. In *Proceedings of 2009 IEEE International Conference on Robotics and Automation*, pages 1479–1484, 2009. 2.3

M.M. Mirbagheri, H. Barbeau, and R.E. Kearney. Intrinsic and reflex contributions to human ankle stiffness: variation with activation level and position. *Experimental Brain Research*, 135:423–436, 2000. ISSN 0014-4819. URL http://dx.doi.org/10.1007/s002210000534. 10.1007/s002210000534. 1.1

NINDS. Tremor fact sheet, June 2006. URL http://www.ninds.nih.gov/disorders/tremor/detail_tremor.htm. [Accessed 18 October 2011] National Institute of Neurological Disorders and Stroke - National Institutes of Health Publication No. 06-4734. 1.1

A. Otten, W. van Vuuren, A. Stienen, E. van Asseldonk, A. Schouten, and H. van der Kooij. Position and torque tracking: Series elastic actuation versus model-based-controlled hydraulic actuation. In *Rehabilitation Robotics (ICORR), 2011 IEEE International Conference on*, pages 1 –6, 29 2011-july 1 2011. doi: 10.1109/ICORR.2011.5975456. 5.3

Eric Perreault, Robert Kirsch, and Patrick Crago. 'effects of voluntary force generation on the elastic components of endpoint stiffness. *Experimental Brain Research*, 141: 312–323, 2001. ISSN 0014-4819. URL http://dx.doi.org/10.1007/s002210100880. 10.1007/s002210100880. 2.1

James B Rowe and Richard SJ Frackowiak. The impact of brain imaging technology on our understanding of motor function and dysfunction. *Current Opinion in Neurobiology*, 9(6):728 – 734, 1999. ISSN 0959-4388. doi: 10.1016/S0959-4388(99)00025-2. URL http://www.sciencedirect.com/science/article/pii/S0959438899000252. 5.4

G. Schaefers. Testing mr safety and compatibility. *Engineering in Medicine and Biology Magazine, IEEE*, 27(3):23 –27, may-june 2008. ISSN 0739-5175. doi: 10.1109/EMB.2007.910267. 2.1

Alfred C. Schouten, Erwin de Vlugt, J.J.Bob van Hilten, and Frans C.T. van der Helm. Design of a torque-controlled manipulator to analyse the admittance of the wrist joint. *Journal of Neuroscience Methods*, 154(12):134 – 141, 2006. ISSN 0165-0270. doi: 10.1016/j.jneumeth.2005.12.001. URL http://www.sciencedirect.com/science/article/pii/S0165027005004498. 2.1, 4

Dan Stoianovici, Alexandru Patriciu, Doru Petrisor, Dumitru Mazilu, and Louis Kavoussi. A new type of motor: Pneumatic step motor. *Mechatronics, IEEE/ASME Transactions on*, 12(1):98 –106, feb. 2007. ISSN 1083-4435. doi: 10.1109/TMECH.2006.886258. 2.2

Nikolaos V. Tsekos, Alpay Ozcan, and Eftychios Christoforou. A prototype manipulator for magnetic resonance-guided interventions inside standard cylindrical magnetic resonance imaging scanners. *Journal of Biomechanical Engineering*, 127(6):972–980, 2005. doi: 10.1115/1.2049339. URL http://link.aip.org/link/?JBY/127/972/1. 2.1, 3.1

Nikolaos V. Tsekos, Azadeh Khanicheh, Eftychios Christoforou, and Constantinos Mavroidis. Magnetic resonancecompatible robotic and mechatronics systems for image-guided interventions and rehabilitation: A review study. *Annual Review of Biomedical Engineering*, 9(1):351–387, 2007. doi: 10.1146/annurev.bioeng.9.121806.160642. URL http://www.annualreviews.org/doi/abs/10.1146/annurev.bioeng.9.121806.160642. 5.4

N.V. Tsekos, E. Christoforou, and A. Ozcan. A general-purpose mr-compatible robotic system. *Engineering in Medicine and Biology Magazine, IEEE*, 27(3):51 –58, may-june 2008. ISSN 0739-5175. doi: 10.1109/EMB.2007.910270. 2.2

Frans C.T. van der Helm, Alfred C. Schouten, Erwin de Vlugt, and Guido G. Brouwn. Identification of intrinsic and reflexive components of human arm dynamics during postural control. *Journal of Neuroscience Methods*, 119(1):1 – 14, 2002. ISSN 0165-0270. doi: 10.1016/S0165-0270(02)00147-4. URL http://www.sciencedirect.com/science/article/pii/S0165027002001474. 1.1

M.P. Vlaar. Design of a fmri-compatible force sensor. Internship report, 2011. 3.2.1

Gregor K Wenning, Stefan Kiechl, Klaus Seppi, Joerg Muller, Birgit Hogl, Michael Saletu, Gregor Rungger, Arno Gasperi, Johann Willeit, and Werner Poewe. Prevalence of movement disorders in men and women aged 5089 years (bruneck study cohort): a population-based study. *The Lancet Neurology*, 4(12):815–820, december 2005. doi: 10.1016/S1474-4422(05)70226-X. 1.1

D. Williams. Robot for wrist rehabilitation'. Master's thesis, MIT, 2001. 2.1

A. Yamamoto, K. Ichiyanagi, T. Higuchi, H. Imamizu, R. Gassert, M. Ingold, L. Sache, and H. Bleuler. Evaluation of mr-compatibility of electrostatic linear motor. In *Robotics and Automation, 2005. ICRA 2005. Proceedings of the 2005 IEEE International Conference on*, pages 3658 – 3663, april 2005. doi: 10.1109/ROBOT.2005.1570677. 2.2

Ningbo Yu, W. Murr, A. Blickenstorfer, S. Kollias, and R. Riener. An fmri compatible haptic interface with pneumatic actuation. In *Rehabilitation Robotics, 2007. ICORR 2007. IEEE 10th International Conference on*, pages 714 –720, june 2007. doi: 10.1109/ICORR.2007.4428504. 2.3

Ningbo Yu, C. Hollnagel, A. Blickenstorfer, S.S. Kollias, and R. Riener. Comparison of mri-compatible mechatronic systems with hydrodynamic and pneumatic actuation. *Mechatronics, IEEE/ASME Transactions on*, 13(3):268 –277, june 2008. ISSN 1083-4435. doi: 10.1109/TMECH.2008.924041. 2.2, 2.3, 5.4